Morphodynamic analysis of coastal areas using numerical models and field data

Vasilia Finikianaki

Department of Mathematics & Applied Mathematics
University of Crete

Thesis
submitted for the degree
Master of Science

July 2016

Acknowledgement

I would like to express my gratitude to my supervisor Nikolaos Kampanis, head director of the Coastal Research Lab - IACM for the useful comments, remarks and support through the learning process of this master thesis.

Furthermore, I would like to thank Dr. George Alexandrakis for introducing me to the topic as well for the support on the way and Professor Serafim Poulos for sharing the field data and observations with me.

Also, I like to thank Dr. George Kozyrakis and Dr. Katerina Spanoudaki for their help.

I would like also to thank the Department of Mathematics and my professors for the opportunities and the knowledge they gave me and especially Professor V. Dougalis and Professor M. Taroudakis for participating in my committee and for their useful remarks.

Finally, I thank my family and my friends who have supported me throughout entire process, both by keeping me harmonious and helping me putting pieces together. I will be grateful forever for your love and support.

To my grandfather
Vasilis Xatziyannis

Abstract

Wind - induced waves are the dominant active phenomenon of the coastal area and have a large influence on the suspension and the transport of sediments in the nearshore area. The wave breaking with the associated wave - induced currents can bring relatively large quantities of sand into suspension which is then transported following the current direction. Although sediment in the nearshore area is moving constantly, transport is a phenomenon based mainly upon extreme events such as storm surges.

In this study, the effect of a strong meteorological event, known as Meltemi, which took place from 24th to 30th July 2003 and monitored at Gouves beach (Poulos et al 2012, 2013) has been simulated and forecasted, using the Delft3D model. The concentration of the suspended sediment near the bed due to the combined effect of the wave - induced currents and the hydrodynamic conditions caused by the storm is computed. In particular, the interaction between waves and currents obtained by the coupling of two models included in Delft3d, the Delft3d - FLOW, for the hydrodynamic computations and the sediment transport processes, and the Delft3d - WAVE, for the computation of the wave field. The two models have been coupled in an appropriate form through communicative artificial boundaries and well chosen boundary conditions, hierarchical grids (nested grids) and appropriate modeling of the outer problem. The results were, also, compared with measurements obtained during the event by Poulos et al. (2012, 2013).

The results of the modeling fit well enough with the measured data. In particular, the model slightly overestimates the significant wave height and the current velocity in the nearshore area and the suspended sediment concentration near the bed at the observation points. However, generally the results of the simulation are very close to the measurements and the different bars formed by erosion and sedimentation are represented with enough accuracy.

Contents

Chapter 1

Introduction

Sediment transport is of crucial importance for coastal environments. It generally occurs under the combined influence of a variety of hydrodynamic processes such as winds, waves and currents. Wind - induced waves are the dominant active phenomenon of the coastal area and have a large influence on the suspension and the transport of sediments in the nearshore area.

Sediments can be transported by waves through wave breaking and the associated wave - induced currents in the long -shore and cross - shore directions. The long - shore transport in the surf zone is also known as the long - shore drift. The breaking process together with the near - bed, wave - induced oscillatory water motion can bring relatively large quantities of sand into suspension (stirring) which is then transported as suspended load by the currents. Although sediment in the near - shore area is moving constantly, transport is a phenomenon based mainly upon extreme events such as storm surges.

In the present study, the effect of the meteorological event, known as *Meltemi*, is simulated and forecasted using a modeling procedure within the Delft3D model, in relation with the characteristics of the waves and currents that induces and the sediment transport that may cause.

The term *Meltemi* refers to the Etesian winds in the Aegean Sea. The Etesian winds are the prevailing annually recurring summer winds, blowing over large parts of Greece, the Aegean Sea and eastern Mediterranean. The Etesian winds blow from a high pressure ridge over the Balkans, towards a heat trough over the Anatolian Plateau (figure 1.1). They appear at the beginning of May with low but also fluctuating frequency and with short duration, and they preserve their character until the end of June. From the beginning of July, the frequency of Etesians increases reaching its greatest values towards the end of the month, which it then preserves until about mid-September, and then reduces at the end of October. The typical weather that is associated with a Meltemi event is dry with clear skies. The strong meteorological conditions caused during such an event have a large influence upon the sediment transport in northern Crete.

In the summer of 2003, a study was performed (Poulos *et. al.*, 2012, Poulos *et. al.*, 2013) at the Gouves coastal area in order to investigate the significance of this event upon the sediment transport in Northern Crete, utilizing measurements about turbidity, current speed and direction and other wave characteristics. The data set has been collected by three Autonomous Benthic Recorders (ABR) placed at three different locations. Also, information about the offshore wave conditions, the bathymetry of the area and meteorological data were collected. The

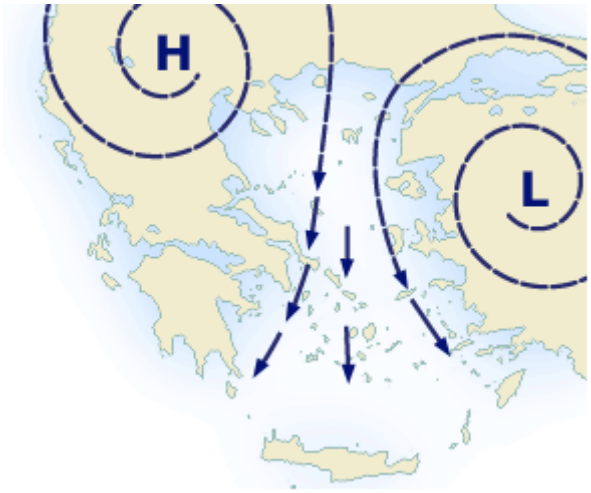

Figure 1.1: Etesian Winds, *www.sailingissues.com*

research took place from the 24th to 30th of July, i.e. before, during and after a strong Meltemi event.

In this study, the Meltemi event and its influence to the sediment transport processes is numerically reproduced, for the period from the 24th to 30th of July 2003, in the area under consideration. Furthermore, the results are compared with the measurements obtained by (Poulos *et. al.*, 2012, Poulos *et. al.*, 2013). The main objectives are to:

- Fine tune the coupling of the particular models included in Delft3D, regarding the appropriate selection of the artificial boundaries and its conditions, the hierarchy of nested grids and appropriate modeling of the outer wave problem.
- Estimate the hydrodynamic conditions of the event.
- Estimate the accuracy of the numerical modeling in relation with the real data.

For the simulation, the numerical model of the open source code of Delft3D was used. With Delft3d, the calculation of the wave field in relation with the hydrodynamics and the sediment transport which depend on the wind field is the product of the coupling of two models, that of the Delft3d - WAVE model (Wave, User Manual) and that of the Delft3d - FLOW model (Flow, User Manual).

This study is presented in the subsequent chapters as follows: In chapter 2, a brief description of the Delft3D model is given. In chapter 3, the case study and the model setup are described. In chapter 4, the results of the computations are presented and, in chapter 5, they are compared with the measurements obtained from the study of (Poulos *et. al.*2012, Poulos *et. al.*2013). Finally, in chapter 6, the conclusions are discussed.

Chapter 2

A brief description of the Delft3D model

The Delft3D module is developed for a multi-disciplinary approach to nearshore waves and morphodynamic modeling by Deltares [1], in close cooperation with Delft University of Technology. Delft3D consists of several models that can interact with each other. The Delft3D - FLOW simulates the hydrodynamic phenomena, the sediment transport processes and the bottom changes and the Delft3D - WAVE simulates the wave generation and propagation in nearshore areas.

In this study, the wave-driven longshore currents and the sediment transport in the surf zone are modeled by the interaction between Delft3D-FLOW and Delft3D-WAVE . The coupling of those models allow a two way exchange of information between them, so as the effect of waves on currents and the effect of flow on waves to be accounted for. More specifically, the wave - current interaction is implemented by running the wave module every N flow timesteps, where updated bottom, water level and velocity information are passed to the wave model and wave - induced forces, wave heights, periods and directions are passed back to the flow module (Lesser *et. al.*, 2004).

2.1 The Delft3D - FLOW model

2.1.1 Shallow water equations

The Delft3D-FLOW model solves the unsteady shallow-water equations for an incompressible fluid. They are derived from the Navier - Stokes equations under the Boussinesq and the shallow water assumptions.

According to the Boussinesq approximation (Rodi, 1993), if density variations are small the density is assumed constant in all terms except the gravitational term. Under this approximation, the Navier - Stokes equations are written in the form: .

$$\begin{aligned} \frac{\partial u}{\partial t} + u\frac{\partial u}{\partial x} + v\frac{\partial u}{\partial y} + w\frac{\partial u}{\partial z} &= -\frac{1}{\rho_0}\frac{\partial p}{\partial x} + \nu\Delta u - f_x \\ \frac{\partial v}{\partial t} + u\frac{\partial v}{\partial x} + v\frac{\partial v}{\partial y} + w\frac{\partial v}{\partial z} &= -\frac{1}{\rho_0}\frac{\partial p}{\partial y} + \nu\Delta v - f_y \end{aligned} \tag{2.1}$$

[1] Deltares is an independent institute for applied research in the field of water and subsurface

$$\frac{\partial w}{\partial t} + u\frac{\partial w}{\partial x} + v\frac{\partial w}{\partial y} + w\frac{\partial w}{\partial z} = -\frac{1}{\rho_0}\frac{\partial p}{\partial z} + \nu\Delta w - f_z - \frac{\rho}{\rho_0}g$$

where u,v,w are the velocity components in x, y and z direction respectively, ρ is the density, ρ_0 is the reference density, p is the pressure, ν the kinematic viscosity and f_x,f_y, f_z denote the components of the Coriolis forces per unit mass, which are defined by:

$$(f_x, f_y, f_z)^T = -2\vec{\Omega} \times (u, v, w)^T$$

where $\vec{\Omega}$ is the vector of the earth's rotation.

In the flow velocities and pressure, small variations occur due to turbulence eddies. These variations are usually too small to be represented in a numerical scheme unless the grid is very fine. In order to deal with this phenomenon, (Reynolds, 1894) decomposed the time - dependent variables into two parts:

$$u = \overline{u} + u',\ v = \overline{v} + v',\ w = \overline{w} + w',\ p = \overline{p} + p',\ f = \overline{f} + f' \tag{2.2}$$

that of the time-averaged part (main flow) denoted by the bar and that of the turbulent fluctuations given by the ' of the quantity. Then, the entire equation is time averaged.

A time-averaged quantity $\overline{q}$ for a flow quantity q is defined as :

$$\overline{q} = \frac{1}{T}\int_t^{t+T} q d\tau$$

The period T should be larger than the turbulence time scale, but smaller than long periodic effects such as the tide.

After averaging 2.1, the Reynolds-averaged Navier-Stokes equations or simply the Reynolds equations for turbulent flows are obtained. They read:

$$\frac{\partial \overline{u}}{\partial t} + \overline{u}\frac{\partial \overline{u}}{\partial x} + \overline{v}\frac{\partial \overline{u}}{\partial y} + \overline{w}\frac{\partial \overline{u}}{\partial z} + \frac{\partial \overline{u'u'}}{\partial x} + \frac{\partial \overline{u'v'}}{\partial y} + \frac{\partial \overline{u'w'}}{\partial z} = -\frac{1}{\rho_0}\frac{\partial \overline{p}}{\partial x} - \overline{f_x} \tag{2.3}$$

$$\frac{\partial \overline{v}}{\partial t} + \overline{u}\frac{\partial \overline{v}}{\partial x} + \overline{v}\frac{\partial \overline{v}}{\partial y} + \overline{w}\frac{\partial \overline{v}}{\partial z} + \frac{\partial \overline{v'u'}}{\partial x} + \frac{\partial \overline{v'v'}}{\partial y} + \frac{\partial \overline{v'w'}}{\partial z} = -\frac{1}{\rho_0}\frac{\partial \overline{p}}{\partial y} - \overline{f_y} \tag{2.4}$$

$$\frac{\partial \overline{w}}{\partial t} + \overline{u}\frac{\partial \overline{w}}{\partial x} + \overline{v}\frac{\partial \overline{w}}{\partial y} + \overline{w}\frac{\partial \overline{w}}{\partial z} + \frac{\partial \overline{w'u'}}{\partial x} + \frac{\partial \overline{w'v'}}{\partial y} + \frac{\partial \overline{w'w'}}{\partial z} = -\frac{1}{\rho_0}\frac{\partial \overline{p}}{\partial z} - \overline{f_z} - \frac{\rho}{\rho_0}g \tag{2.5}$$

The products of the fluctuating velocity components ($\overline{u'u'}$,$\overline{u'v'}$ etc.) are called Reynolds stresses and they are responsible for a loss of momentum in the mean flow direction. These stresses are much larger than the viscous stresses which have, therefore, been neglected.

Furthermore, according to the Boussinesq hypothesis (eddy viscosity concept), Reynolds stresses, like viscous stresses, depend on the deformation of the mean flow. Thus, the Reynolds stresses can be modeled as

$$\overline{u'v'} = -\nu_t\left(\frac{\partial \overline{v}}{\partial x} + \frac{\partial \overline{u}}{\partial y}\right) \tag{2.6}$$

where ν_t is the eddy viscosity and is determined with a suitable closure problem for the turbulence modelling.

The *shallow water* assumption implies that the flow satisfies certain characteristic relations (Jin, 1993). These relations are the following :

1. The characteristic horizontal length scale is much larger than the characteristic vertical length scale.

2. The characteristic vertical velocity is small in comparison with the characteristic horizontal velocity.

Under this assumption, the difference between the horizontal and the vertical length scale justifies a distinction between a horizontal (ν_t^H) and a vertical (ν_t^V) eddy viscosity. Also, all the terms except the pressure derivative and the gravity term are small, so they can be neglected. The momentum equation in the vertical direction reduces to the hydrostatic pressure distribution:

$$\frac{\partial \overline{p}}{\partial z} = -\rho g \tag{2.7}$$

i.e. by integrating

$$\overline{p}(x, y, z, t) = g \int_z^{\zeta} \rho dz' + p_a \tag{2.8}$$

where $\zeta = \zeta(x, y, t)$ is the free surface level against the reference plane $z = 0$ and p_a is the atmospheric pressure. Substituting this result in the pressure term of equation 2.3 and using Leibnitz' integration rule [1], yields

$$-\frac{1}{\rho_0}\frac{\partial \overline{p}}{\partial x} = -\frac{\rho g}{\rho_0}\frac{\partial \zeta}{\partial x} - \frac{g}{\rho_0}\int_z^{\zeta} \frac{\partial \rho}{\partial x} dz' - \frac{1}{\rho_0}\frac{\partial p_a}{\partial x} \tag{2.9}$$

The horizontal pressure gradient is described by differences of the water level ζ through the barotropic term (gradient of the free surface level) and by the density differences in horizontal direction through the baroclinic term (second term). The last term describes the contribution of the atmospheric pressure.

If we consider $\rho = \rho_0$ (constant), then (2.8) reads as $\overline{p} = \rho g(\zeta - z) + p_a$ and for the pressure terms of (2.3) and (2.4) we have

$$\frac{1}{\rho_0}\frac{\partial \overline{p}}{\partial x} = g\frac{\partial \zeta}{\partial x} + \frac{1}{\rho_0}\frac{\partial p_a}{\partial x} \tag{2.10}$$

and

$$\frac{1}{\rho_0}\frac{\partial \overline{p}}{\partial y} = g\frac{\partial \zeta}{\partial y} + \frac{1}{\rho_0}\frac{\partial p_a}{\partial y} \tag{2.11}$$

respectively.

[1] The Leibnitz' integration rule:

$$\frac{\partial}{\partial x}\int_{a(x)}^{b(x)} \phi(x, y)dy = \int_{a(x)}^{b(x)} \frac{\partial}{\partial x}\phi(x, y)dy + \phi(x, b)\frac{\partial b}{\partial x} - \phi(x, a)\frac{\partial a}{\partial x}$$

Considering the above assumptions, the density and the atmospheric pressure to be constant and dropping the overbar, equations (2.3) and (2.4) are, respectively, transformed into:

$$\frac{\partial u}{\partial t}+u\frac{\partial u}{\partial x}+v\frac{\partial u}{\partial y}+w\frac{\partial u}{\partial z}=-g\frac{\partial \zeta}{\partial x}+fv+2\frac{\partial\left(\nu_t^H\frac{\partial u}{\partial x}\right)}{\partial x}+\frac{\partial\left(\nu_t^H\left(\frac{\partial u}{\partial y}+\frac{\partial v}{\partial x}\right)\right)}{\partial y}+\frac{\partial\left(\nu_t^V\frac{\partial u}{\partial z}\right)}{\partial z} \quad (2.12)$$

$$\frac{\partial v}{\partial t}+u\frac{\partial v}{\partial x}+v\frac{\partial v}{\partial y}+w\frac{\partial v}{\partial z}=-g\frac{\partial \zeta}{\partial y}-fu+\frac{\partial\left(\nu_t^H\left(\frac{\partial u}{\partial y}+\frac{\partial v}{\partial x}\right)\right)}{\partial x}+2\frac{\partial\left(\nu_t^H\frac{\partial v}{\partial y}\right)}{\partial y}+\frac{\partial\left(\nu_t^V\frac{\partial v}{\partial z}\right)}{\partial z} \quad (2.13)$$

where f is the *Coriolis* force, defined as

$$f=2\Omega\sin\phi$$

with Ω to represent the angular velocity of the earth and ϕ the latitude.

The above equations together with the incompressible continuity equation

$$\frac{\partial u}{\partial x}+\frac{\partial v}{\partial y}+\frac{\partial w}{\partial z}=0 \quad (2.14)$$

are the so-called *Shallow Water Equations*.

In order to obtain the fourth equation that is needed for calculating the four unknowns (u,v,w,ζ), the continuity equation is integrated along the vertical axis :

$$w(x,y,\zeta,t)-w(z,y,d,t)=-\int_{-d}^{\zeta}\frac{\partial u}{\partial x}dz-\int_{-d}^{\zeta}\frac{\partial v}{\partial y}dz \quad (2.15)$$

where $d=d(x,y)$ is the water depth below the reference plane $z=0$. For the water level ($z=\zeta(x,y,t)$) and for the bottom ($z=-d(x,y)$) respectively,

$$w=\frac{D\zeta}{Dt}=\frac{\partial\zeta}{\partial t}+u\frac{\partial\zeta}{\partial x}+v\frac{\partial\zeta}{\partial y} \quad (2.16)$$

$$w=-u\frac{\partial d}{\partial x}-v\frac{\partial d}{\partial y} \quad (2.17)$$

Using the Leibnitz' rule,

$$-\int_{-d}^{\zeta}\frac{\partial u}{\partial x}dz=-\frac{\partial}{\partial x}\int_{-d}^{\zeta}udz+u\frac{\partial\zeta}{\partial x}+u\frac{\partial d}{\partial x}$$

and

$$-\int_{-d}^{\zeta}\frac{\partial v}{\partial y}dz=-\frac{\partial}{\partial y}\int_{-d}^{\zeta}vdz+v\frac{\partial\zeta}{\partial y}+v\frac{\partial d}{\partial y}$$

(2.15) yields:

$$\frac{\partial\zeta}{\partial t}=-\frac{\partial}{\partial x}\int_{-d}^{\zeta}udz-\frac{\partial}{\partial y}\int_{-d}^{\zeta}vdz \quad (2.18)$$

Finally, defining the depth-averaged velocities $\bar{u}$ and $\bar{v}$ by $\bar{u}=\frac{1}{H}\int_{-d}^{\zeta}udz$ and $\bar{v}=\frac{1}{H}\int_{-d}^{\zeta}vdz$ respectively, where $H=H(x,y,t)=\zeta+d$ is the water depth, equation (2.18) is written in the form:

$$\frac{\partial\zeta}{\partial t}+\frac{\partial H\bar{u}}{\partial x}+\frac{\partial H\bar{v}}{\partial y}=0 \quad (2.19)$$

The hydrodynamic equations are solved on a Cartesian, rectangular grid. In 3D simulations, a boundary fitted (σ - coordinate) approach is used for the vertical grid direction.

The σ coordinate system is a boundary fitted coordinate system that follows the free surface and the bottom topography. Such a coordinate system allows for non - uniformly distributed grid lines on the computational domain, especially near the bottom, where a proper forecasting of the sediment transport requires the grid lines to be dense and therefore to increase the resolution.

In the following, the complex physical domain for the shallow water equations 2.12, 2.13, 2.14 and 2.19 is transformed to a rectangular computational domain by introducing the σ-coordinates system

$$\tilde{x} = x, \quad \tilde{y} = y, \quad \sigma = \frac{z - \zeta}{H}, \quad \tilde{t} = t \tag{2.20}$$

where:

z = the vertical coordinate in physical space

ζ = the free surface elevation above the reference plane ($z = 0$)

d = the depth below the reference plane

H = the total water depth , given by $H = d + \zeta$

At the bottom $\sigma = -1$ and at the free surface $\sigma = 0$. The flow domain of a 3D shallow water model in the horizontal plane consists of a restricted (limited) area composed of open and closed (land) boundaries and in the vertical of a number of layers, which is the same at every location. For each layer, a system of equations is solved.

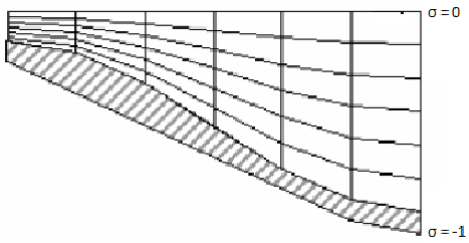

Figure 2.1: An example of a vertical grid consisting of six equal thickness σ - layers, *Delft3D - Flow, User Manual (2014)*

The partial derivatives are expressed in σ - coordinates by the chain rule, introducing additional terms (Stelling *et. al.*, 1994).

The time derivative in σ-coordinates reads:

$$\frac{\partial}{\partial t} = \frac{\partial}{\partial \tilde{t}} + \frac{\partial \sigma}{\partial \tilde{t}} \frac{\partial}{\partial \sigma}$$

The spatial derivatives in the horizontal direction are:

$$\frac{\partial}{\partial x} = \frac{\partial}{\partial \tilde{x}} + \frac{\partial \sigma}{\partial \tilde{x}} \frac{\partial}{\partial \sigma}, \quad \frac{\partial}{\partial y} = \frac{\partial}{\partial \tilde{y}} + \frac{\partial \sigma}{\partial \tilde{y}} \frac{\partial}{\partial \sigma}$$

In the vertical direction:

$$\frac{\partial}{\partial z} = \frac{1}{H} \frac{\partial}{\partial \sigma}$$

Equation 2.7 in σ- coordinates reads:

$$\frac{\partial \tilde{p}}{\partial \sigma} = -\rho g H \tag{2.21}$$

After integrating along the vertical axis we obtain the hydrostatic pressure :

$$\tilde{p} = gH \int_{\sigma}^{0} \rho(x, y, \sigma, t) d\sigma' + p_a \tag{2.22}$$

The horizontal velocities u and v remain strictly horizontal after the transformation

$$\tilde{u} = u, \quad \tilde{v} = v$$

whereas, the vertical velocity becomes

$$\tilde{\omega} := H \frac{D\sigma}{D\tilde{t}}$$

$$\tilde{\omega} = H \left[\frac{\partial}{\partial t} \left(\frac{z - \zeta}{H} \right) + u \frac{\partial}{\partial x} \left(\frac{z - \zeta}{H} \right) + \frac{\partial}{\partial y} \left(\frac{z - \zeta}{H} \right) \right]$$

$$\tilde{\omega} = w - \left(\frac{\partial \zeta}{\partial t} + u \frac{\partial \zeta}{\partial x} + v \frac{\partial \zeta}{\partial y} \right) - \sigma \left(\frac{\partial H}{\partial t} + u \frac{\partial H}{\partial x} + v \frac{\partial H}{\partial y} \right) \tag{2.23}$$

From this, the (comparatively small) vertical velocity w can be expressed in the (x,y,z) coordinates, in terms of the horizontal velocities, water depths, water levels and vertical σ - velocities, as

$$w = \tilde{\omega} + u \left(\sigma \frac{\partial H}{\partial x} + \frac{\partial \zeta}{\partial x} \right) + v \left(\sigma \frac{\partial H}{\partial y} + \frac{\partial \zeta}{\partial y} \right) + \left(\sigma \frac{\partial H}{\partial t} + \frac{\partial \zeta}{\partial t} \right)$$

After substituting (2.23) into the continuity equation (2.14), assuming that d is not time-dependent and noting that H and ζ are not σ-dependent, whereas u and v are, the continuity equation in transformed coordinates is obtained:

$$\frac{\partial \zeta}{\partial \tilde{t}} + \frac{\partial H \tilde{u}}{\partial \tilde{x}} + \frac{\partial H \tilde{v}}{\partial \tilde{y}} + \frac{\partial \omega}{\partial \sigma} = 0 \tag{2.24}$$

The vertical velocities can be computed by integrating equation 2.24 from the bottom to the surface ($-1 \leq \sigma \leq 0$) and using Leibnitz' integration rule:

$$\frac{\partial \zeta}{\partial \tilde{t}} + \frac{\partial H \bar{u}}{\partial \tilde{x}} + \frac{\partial H \bar{v}}{\partial \tilde{y}} = 0 \tag{2.25}$$

where $\bar{u}$ and $\bar{v}$ are depth-averaged velocities defined by $\bar{u} = \int_{-1}^{0} \tilde{u} d\sigma$ and $\bar{v} = \int_{-1}^{0} \tilde{v} d\sigma$. Note that, this equation is equal to (2.19) in the previous section, because it is integrated along the vertical axis and therefore invariant under the σ-transformation. Also, the definitions of $\bar{u}$ and $\bar{v}$ are equivalent to the definitions in the previous section.

After transformation of (2.12) and (2.13) to σ-coordinates, the momentum equations in x- and y-direction of the shallow-water equations, omitting the overbar, are given by:

$$\frac{\partial u}{\partial t}+u\frac{\partial u}{\partial x}+v\frac{\partial u}{\partial y}+\frac{\omega}{H}\frac{\partial u}{\partial \sigma}=-\frac{1}{\rho_0}\left(\frac{\partial p}{\partial x}+\frac{\partial \sigma}{\partial x}\frac{\partial p}{\partial \sigma}\right)+fv+F_x+M_x+\frac{1}{H^2}\frac{\partial}{\partial \sigma}\left(\nu_t^V\left(\frac{\partial u}{\partial \sigma}\right)\right) \quad (2.26)$$

$$\frac{\partial v}{\partial t}+u\frac{\partial v}{\partial x}+v\frac{\partial v}{\partial y}+\frac{\omega}{H}\frac{\partial v}{\partial \sigma}=-\frac{1}{\rho_0}\left(\frac{\partial p}{\partial y}+\frac{\partial \sigma}{\partial y}\frac{\partial p}{\partial \sigma}\right)+fu+F_y+M_y+\frac{1}{H^2}\frac{\partial}{\partial \sigma}\left(\nu_t^V\left(\frac{\partial v}{\partial \sigma}\right)\right) \quad (2.27)$$

$$\frac{\partial \zeta}{\partial t}+\frac{\partial Hu}{\partial x}+\frac{\partial Hv}{\partial y}+\frac{\partial \omega}{\partial \sigma}=0 \quad (2.28)$$

The terms M_x and M_y are introduced to represent the contributions due to external sources or sinks of momentum (external forces by hydraulic structures, discharge or withdrawal of water, wave stresses, etc.).

The terms F_x and F_y represent the horizontal viscosity terms and they are given by:

$$F_x=\nu_H\left(\frac{\partial^2 u}{\partial x^2}+\frac{\partial^2 u}{\partial y^2}\right) \quad and \quad F_y=\nu_H\left(\frac{\partial^2 v}{\partial x^2}+\frac{\partial^2 v}{\partial y^2}\right) \quad (2.29)$$

where the horizontal eddy viscosity has been assumed to be a constant.

2.1.2 Boundary Conditions

To get a well-posed mathematical problem with a unique solution, a set of initial and boundary conditions for water levels and horizontal velocities must be specified. The contour of the model domain consists of parts along land-water lines (coast lines) which are called closed boundaries and parts across the flow field which are called open boundaries. Closed boundaries are natural boundaries. The velocities normal to a closed boundary are set to zero (Flow, User Manual).

2.1.2.1 Vertical Boundary Conditions

Kinematic Boundary Conditions:

In the σ coordinate system, the free surface ($\sigma = 0$, or $z = \zeta$) and the bottom ($\sigma = -1$, or $z = -d$) are σ - coordinate surfaces. The impermeability of the surface and the bottom is taken into account by prescribing the following kinematic conditions:

$$\omega|_{\sigma=-1} = 0 \;\; and \;\; \omega|_{\sigma=0} = 0 \tag{2.30}$$

where ω is the vertical velocity relative to the σ - plane.

Bed Boundary Condition:

At the seabed, the boundary conditions for the momentum equations are:

$$\left.\frac{\nu_V}{H}\frac{\partial u}{\partial \sigma}\right|_{\sigma=-1} = \frac{\tau_{bx}}{\rho_0} \tag{2.31}$$

$$\left.\frac{\nu_V}{H}\frac{\partial v}{\partial \sigma}\right|_{\sigma=-1} = \frac{\tau_{by}}{\rho_0} \tag{2.32}$$

where τ_{bx} and τ_{by} are the components of the bed stress in x and y direction, respectively, that include the effects of wave - current interaction. Their formulation for the combination of flow and wave will be discussed later.

The bed shear stress in 3D is related to the current just above the bed:

$$\vec{\tau}_{b3D} = \frac{g\rho_0 \vec{u_b}|\vec{u_b}|}{C_{3D}^2} \tag{2.33}$$

where $|\vec{u_b}|$ is the magnitude of the horizontal velocity in the first layer just above the bed and C_{3D} is the Chézy coefficient (Flow, User Manual).

Surface Boundary Condition:

At the free surface the boundary conditions for the momentum equations are:

$$\left.\frac{\nu_V}{H}\frac{\partial u}{\partial \sigma}\right|_{\sigma=0} = \frac{|\vec{\tau_s}|}{\rho_0}\cos(\theta) \tag{2.34}$$

$$\left.\frac{\nu_V}{H}\frac{\partial u}{\partial \sigma}\right|_{\sigma=0} = \frac{|\vec{\tau_s}|}{\rho_0}\sin(\theta) \tag{2.35}$$

where θ is the angle between the wind stress vector and the local direction of the grid line y is constant. Without wind, the stress at the free surface is zero. The magnitude of the wind shear - stress is defined as:

$$|\vec{\tau_s}| = \rho_0 \vec{u}_{*s} |\vec{u_{*s}}| \tag{2.36}$$

where u_{*s} is the friction velocity at the free surface and it can be determined by the following widely used quadratic expression:

$$|\vec{\tau_s}| = \rho_\alpha C_d {U_{10}}^2 \tag{2.37}$$

where:

ρ_α the air density

U_{10} the wind speed 10 meter above the free surface

C_d the wind drag coefficient, depending on U_{10}

2.1.2.2 Open Boundaries and artificial conditions

Open boundaries are artificial, water-water boundaries. They are situated as far away as possible from the area of interest and they are introduced to obtain a limited computational area and so to reduce the computational effort.

In general, the boundary conditions are specified in a limited number of boundary points. Linear interpolation is used to generate the boundary conditions at the intermediate points along the boundary. This interpolation can generate physical unrealistic flows in the region close to the open boundary. The boundary conditions should allow these disturbances to propagate out of the area. Alternatively, the number of points where the boundary condition is specified should be extended.

For the needs of this study, we follow (Roelvink *et. al.*, 2004). According to this paper, one main problem is the specification of suitable boundary conditions at the open boundaries. This is due to a combination of processes acting on the model domain, resulting in the development of a certain water level or velocity in the cross - shore direction. For the boundary conditions to match this distribution the solution has to be known beforehand, otherwise boundary disturbances will develop.

In order to overcome this problem, (Roelvink *et. al.*, 2004)suggest to let the model determine the correct solution at the boundaries by imposing the alongshore water level gradient (a so-called Neumann boundary condition) instead of a fixed water level or velocity. In this case, it is assumed to be zero. Neumann boundaries can only be applied on cross-shore boundaries in combination with a water level boundary, $\zeta = F_\zeta(t)$, which is needed to make the solution of the mathematical boundary value problem well - posed.

2.1.2.3 Closed Boundaries

A closed boundary is situated at the transition between land and water. At a closed boundary, two boundary conditions have to be prescribed. One boundary condition has to do with the flow normal to the boundary and the other one with the shear-stress along the boundary. The boundary condition considered for flow normal to the boundary is that there is no flow through

the boundary. For the shear stress along the boundary a zero tangential shear-stress (free slip) has been prescribed.

2.2 Sediment transport

The suspended load transport is the irregular motion of the particles through the water column induced by drag forces due to turbulence that act on the particles.

In the surf zone of sandy beaches the transport is generally dominated by waves through wave breaking and the associated wave-induced currents in the longshore and cross-shore directions. In case that wind is the main force of wave generation, the wind stresses and the wave - induced forces generate currents in the sea, that can both stir up and transport sediments, and hence the sediment transport largely follows the current direction (Soulsby, 1997). The breaking process together with the near-bed, wave-induced oscillatory water motion can bring relatively large quantities of sediment into suspension (stirring) which is then transported as suspended load by the currents.

Also, the nature of the sea bed (plane or rippled) has a fundamental role in the transport of sediments by waves and currents. The configuration of the sea bed controls the near-bed velocity profile, the shear stresses and the turbulence and, thereby, the mixing and transport of the sediment particles.

The transport of bed material particles may be in the form of either bed-load or bed-load plus suspended load, depending on the size of the bed material particles and the flow conditions. When the value of the bed-shear velocity just exceeds the critical value for initiation of motion, the particles will be rolling and sliding or both, in continuous contact with the bed. For increasing values of the bed-shear velocity, the particles will be moving along the bed by more or less regular jumps, which are called saltations. When the value of the bed-shear velocity exceeds the fall velocity of the particles, the sediment particles can be lifted to a level at which the upward turbulent forces will be comparable with or of higher order than the submerged weight of the particles. As a result, the particles may go in suspension.

In particular, particle movement will occur when the instantaneous fluid force on a particle is just larger than the instantaneous resisting force related to the submerged particle weight and the friction coefficient. The degree of exposure of a grain with respect to surrounding grains (hiding of smaller particles resting or moving between the larger particles) obviously is an important parameter determining the forces at initiation of motion.

The fluid forces acting on a sediment particle resting on a horizontal bed consist of skin friction forces and pressure forces. The skin friction force acts on the surface of the particles by viscous shear. The pressure force consisting of a drag and a lift force is generated by pressure differences along the surface of the particle. These forces per unit bed surface area can be reformulated in a time-averaged bed-shear stress.

The initiation of motion is defined to occur when the dimensionless bed-shear stress (θ) is larger than a threshold value (θ_{cr}). This threshold value, which is also referred to as the particle mobility number is defined, according to (Shields, 1936) as:

$$\theta_{cr} = \frac{\tau_b}{(\rho_s - \rho_w) g D_{50}} \tag{2.38}$$

where:

τ_b = bed-shear stress

ρ_s = sediment density

ρ_w = fluid density

D_{50} = median sediment diameter

A more convenient approach is to express the initiation of the motion as a function of the dimensionless particle size D_*. The parameter D_* is defined as:

$$D_* = D_{50} \left[\frac{(s-1)g}{\nu^2} \right]^{1/3} \tag{2.39}$$

where s is the relative density of the sediment and water (ρ_s/ρ_w) and ν is the kinematic viscosity (m^2/s). A simple expression for initiation of motion is given by (Soulsby, 1997):

$$\theta_{cr,motion} = \frac{0.3}{1 + 1.2D_*} + 0.055(1 - \exp(-0.02D_*)) \tag{2.40}$$

Also, a simple expression for initiation of suspension (particles moving in suspension) is given by:

$$\theta_{cr,suspension} = \frac{0.3}{1 + D_*} + 0.1(1 - \exp(-0.05D_*)) \tag{2.41}$$

Both equations can be used to compute the critical depth - averaged velocity for initiation of motion and suspension. Thus, according to (Soulsby, 1997) a simple approximation formula is:

$$U_{cr,motion} = 0.19 D_{50}^{0.1} \log(12H/6D_{50}) \tag{2.42}$$

and

$$U_{cr,suspension} = 2.8 \left[H/D_{50} \right]^{0.1} \left[(s-1)gD_{50} \right]^{0.5} \tag{2.43}$$

In Delft3D - FLOW module, also another model is included which accounts for the three-dimensional transport of the suspended sediment, the Delft3D - SED.

This module solves the three-dimensional advection - diffussion equation for the suspended sediment:

$$\frac{\partial c}{\partial t} + \frac{\partial uc}{\partial x} + \frac{\partial vc}{\partial y} + \frac{\partial (w - w_s)c}{\partial z} +$$
$$- \frac{\partial}{\partial x}\left(\epsilon_{s,x} \frac{\partial c}{\partial x} \right) - \frac{\partial}{\partial y}\left(\epsilon_{s,y} \frac{\partial c}{\partial y} \right) - \frac{\partial}{\partial z}\left(\epsilon_{s,z} \frac{\partial c}{\partial z} \right) = 0 \tag{2.44}$$

where c is the mass concentration of the sediment fraction, $[kg/m^3]$, u, v, w are the flow velocity components $[m/s]$, w_s is the sediment settling velocity, $[m/s]$ and $\epsilon_{s,x}, \epsilon_{s,y}, \epsilon_{s,z}$ are the eddy diffusivities of the sediment fraction $[m^2/s]$.

The settling velocity for a non - cohesive sediment is computed following the Van Rijn's method (Van Rijn, 1993) by the formula

$$w_s = 1.1\sqrt{(s-1)gD_s}, \quad D_s \geq 1000\mu m \tag{2.45}$$

where s is the relative density ρ_s/ρ_w and D_s the representative diameter of the sediment.

2.2.0.1 Initial and Boundary conditions

To solve 2.44 we need to prescribe initial and boundary conditions for the suspended sediment fraction.

One global or space varying initial concentration can be specified for the sediment fraction. In many practical applications the non-cohesive sediment concentrations adapt very rapidly to equilibrium conditions, so in the case of a cold start where the hydrodynamic model also takes some time to stabilize, a uniform zero concentration for the non-cohesive sediment fractions is usually adequate.

A boundary condition must be prescribed for the sediment fraction, for each of the model boundaries.

Water surface boundary: The vertical diffusive flux through the free surface is set to zero for suspended sediment as, also, for all conservative constituents (except heat, which can cross this boundary).

$$-w_s c - \epsilon_{s,z} \frac{\partial c}{\partial z} = 0, \quad at \;\; z = \zeta \tag{2.46}$$

where $z = \zeta$ is the location of the free surface.

Bed boundary condition: The exchange of material in suspension and the bed is modeled by calculating the sediment fluxes from the bottom computational layer to the bed, and vice versa. These fluxes are then applied to the bottom computational layer by means of a sediment source and/or sink term in each computational cell. The calculated fluxes are also applied to the bed in order to update the bed level. The boundary condition at the bed is given by:

$$-w_s c - \epsilon_{s,z} \frac{\partial c}{\partial z} = D - E, \quad at \;\; z = z_b \tag{2.47}$$

where:

D = sediment deposition rate of sediment fraction

E = sediment erosion rate of sediment fraction

Their formulations will be discussed later.

Open inflow boundaries: To assist with modeling coarse material such as sand, we can consider that, at all open inflow boundaries, the flow should enter carrying all sand sediment fractions at their *equilibrium* concentration profiles. This feature has been implemented as a Neumann boundary condition, that is, zero concentration gradient at the boundary. By setting the sediment concentrations at the boundary equal to those just inside the model domain, a near-perfectly adapted flow will enter the domain and very little accretion or erosion should be experienced near the model boundaries. This will generally be the desired situation if the model boundaries are well chosen.

Open outflow boundaries: No boundary condition is prescribed at outflow boundaries; effectively this means that the dispersive transport of sediment at the outflow boundary is neglected compared to the advective transport.

2.2.0.2 Turbulence closure model

For 3D shallow water flow, the horizontal eddy viscosity coefficient ν_H and eddy diffusivity coefficients $\epsilon_{s,x}, \epsilon_{s,y}$ are much larger than the vertical coefficients ν_V and $\epsilon_{s,z}$, i.e. $\nu_H \gg \nu_V$ and $\epsilon_{s,x}, \epsilon_{s,y} \gg \epsilon_{s,z}$. The horizontal coefficients are assumed to be a superposition of three parts:

1. A part due to molecular viscosity. The molecular viscosity of the water is a constant value $O(10)^{-6}$.
2. A part due to 2D-turbulence, which is associated with the contribution of horizontal motions and forcings and its values may either be specified by the user as a constant or space-varying parameter, or can be computed using a sub-grid model for horizontal large eddy simulation (HLES ; Uittenbogaard (1998),Van Vossen (2000))
3. A part due to 3D-turbulence, which is computed by the turbulence closure model, (Uittenbogaard *et. al.*, 1992).

In this study, the k - ϵ model is used to simulate the eddy viscosity and the eddy diffussivity terms in the flow and transport equations.[2]

The k - ϵ model is a second order turbulence closure model, in which, both the turbulence energy k and dissipation rate of turbulent kinetic energy ϵ are calculated by a transport equation. The mixing length L is computed from k and ϵ:

$$L = c_D \frac{k\sqrt{k}}{\epsilon} \tag{2.48}$$

in which c_D is a calibration constant.

The eddy viscosity at each layer interface is determined by:

$$\nu_{3D} = c'_\mu L\sqrt{k} \tag{2.49}$$

where :

c'_μ = a constant determined by calibration, derived for the empirical constant c_μ in the k -ϵ model ; $c'_\mu = c_\mu^{1/4}$, $c_\mu = 0.09$

L = the mixing length

k = the turbulent kinetic energy

The output of the turbulence closure model is the eddy viscosity. From this, the vertical sediment mixing coefficient is computed directly from the vertical fluid mixing coefficient calculated by the turbulence closure model, using the following expressions:

$$\epsilon_s = \beta_{eff}\epsilon_f \tag{2.50}$$

where :

ϵ_s = vertical sediment mixing coefficient of sediment fraction
ϵ_f = vertical fluid mixing coefficient calculated by the k-ϵ turbulent closure model
β_{eff} = the effective Van Rijn's "beta" factor of sediment fraction

[2]For details about the other turbulence closure models see (Flow, User Manual).

As the beta factor should only be applied to the current- related mixing, it is estimated as:

$$\beta_{eff} = 1 + (\beta - 1)\frac{\tau_c}{\tau_w + \tau_c}$$

for non - cohesive sediment fractions, where

τ_c = bed shear stress due to currents
τ_w = bed shear stress due to waves
β = Van Rijn's *beta* factor of the sediment fraction which is calculated from (Van Rijn, 1984b)

$$\beta = 1 + 2\left(\frac{w_s}{u_{*,c}}\right)^2 \tag{2.51}$$

where $u_{*,c}$ is the local bed shear stress due to currents (Van Rijn, 1993)

2.2.0.3 3D Wave effects

In relatively shallow areas (coastal seas) wave action becomes important due to several processes:

- The vertical mixing processes are enhanced due to turbulence generated near the surface by whitecapping and wave breaking, and near the bottom due to energy dissipation in the bottom layer,
- A net mass flux is generated which has some effect on the current profile, especially in the cross-shore direction,
- In the surf zone long-shore currents and a cross-shore set-up is generated due to variations in the wave-induced momentum flux (radiation stress). In case of an irregular surf zone, strong circulations due to bathymetry may be generated (rip currents),

and the most important, related to sediment transport

- The bed shear stress is enhanced; this affects the stirring up of sediments and increases the bed friction. The boundary layers at the bed associated with the waves and the current interact with a non-linear way. This has the effect of enhancing both the mean and oscillatory bed shear-stresses. In addition, the current profile is modified, because the extra turbulence generated close to the bed by the waves appears to the current as being equivalent to an enhanced bottom roughness.

  Various, often very complex, methods exist to describe the bottom boundary layer under combined current and wave action and the resulting virtual roughness. (Soulsby *et. al.*, 1993a) developed a parameterisation of these methods allowing a simple implementation and comparison of various wave-current interaction models: Fredsoe (1984); Myrhaug and Slaattelid (1990); Grant and Madsen (1979); Huynh-Thanh and Temperville (1991); Davies et al. (1988); Bijker (1967); Christoffersen and Jonsson (1985); O Connor and Yoo (1988); Van Rijn et al. (2004). In this study, the method of Grant and Madsen (1979) has been selected.

For a detail description of the mentioned effects above and their mathematical formulation, the interested reader is referred to (Flow, User Manual).

2.3 Numerical aspects

The numerical method of Delft3D-FLOW is based on finite differences. An alternating direction implicit (ADI) method is used to solve the continuity and horizontal momentum equations (Stelling and Leendertse, 1992) extended the ADI method of Leendertse with a special approach for the horizontal advection terms, known as the "cyclic method". The transport equation is formulated in a conservative form (finite - volume approximation) and is solved using the so - called "cyclic method of (Stelling *et. al.*, 1991), including the algorithm of (Stelling *et. al.*, 1994)) for the approximation of the horizontal diffusion along z-planes in a σ - coordinate framework. The reader is referred to (Flow, User Manual) for more details about the numerical methods applied in the Delft3d model.

The time step condition is based on the Courant Friedrichs Lewy (CFL) number for wave propagation:

$$CFL_{wave} = 2\Delta t\sqrt{gH}\sqrt{\frac{1}{\Delta x^2} + \frac{1}{\Delta y^2}} < 1 \tag{2.52}$$

where Δt is the time step, g is the acceleration of gravity, H is the total water depth and Δx,Δy are the smallest grid spaces in x - and y -direction of the physical space.

Chapter 3

The wave model

3.1 Wave height and period

In the description of wind waves it is common to define the wave height H as the vertical distance between the highest and the lowest surface elevation (crest to trough) in a wave. The mean wave height $\overline{H}$ is defined as

$$\overline{H} = \frac{1}{N}\sum_{i=1}^{N} H_i \tag{3.1}$$

where i is the sequence of the wave in a record. Sometimes, a quadratically weighted averaged value is used to define the root - mean - square wave height H_{rms}:

$$H_{rms} = \left(\frac{1}{N}\sum_{i=1}^{N} H_i^2\right)^{1/2} \tag{3.2}$$

which is relevant for energy-related projects because the wave energy is proportional to the square of the wave height.

These characteristic wave heights $\overline{H}$ and H_{rms} they are not very often used because they deviate from visual estimated wave heights. Instead, another wave height, called the significant wave height H_s is used. It is defined as the mean of the highest one - third of waves in a wave record:

$$H_s = H_{1/3} = \frac{1}{N/3}\sum_{j=1}^{N/3} H_j \tag{3.3}$$

where j is the rank number of the sorted wave heights (j=1 the highest wave, j=2 the second - highest, etc.).

The period T of a wave is defined as the time interval between two crests/troughs or two downward/upward zero-crossings. If the wave period is defined as the zero-crossings, it is called T_o and the mean wave period $\overline{T}$ is defined as:

$$\overline{T} = \frac{1}{N}\sum_{i=1}^{N} H_{o,i} \tag{3.4}$$

Mostly, only the significant wave period is used:

$$T_s = T_{1/3} = \frac{1}{N/3}\sum_{j=1}^{N/3} T_{o,j} \tag{3.5}$$

3.2 The Delft3d - WAVE model

The computation of waves and wave-induced effects is the domain of the wave model (Delft3D - WAVE). Delft3D - WAVE supports currently a third generation wave model, namely the SWAN model, that explicitly represents all relevant physics for the development of the sea state in two dimensions (Ris, 1997).

The SWAN model is developed to simulate waves in the near-shore zone. This zone extends from the coast to several tens of kilometers into the sea. Using available input data (wind, current, water velocity), SWAN computes random, short - crested wind-generated waves in coastal regions and inland waters.

3.3 Spectral description of wind waves

Wind generated waves have irregular wave heights and periods, caused by the irregular nature of wind. Due to this irregular nature, the sea surface The surface elevation of waves in the ocean, at any location and any time, can be seen as the superposition of a large number of harmonic waves of different frequencies, each of which has been generated by turbulent wind in different places and times. They are therefore statistically independent in their origin. According to linear wave theory, they remain independent during their journey across the ocean.All these regular wave fields propagate at different speeds so that the appearance of the sea surface is constantly changing. Under these conditions, the sea surface elevation on a time scale of one hundred characteristic wave periods is sufficiently well described as a stationary, Gaussian process. The sea surface elevation in one point as a function of time can be described as

$$\eta(t) = \sum_i a_i \cos(\sigma_i t + \phi_i) \tag{3.6}$$

with η the sea surface elevation, a_i the amplitude of the i^{th} wave component, σ_i the relative radian or circular frequency of the i^{th} wave component in the presence of the ambient current (equals the absolute radian frequency ω when no ambient current is present) and ϕ_i the random phase of the i^{th} wave component. This is called the random-phase model.

In case an ambient current is present, it is assumed that it is uniform with respect to the vertical co-ordinate and the changes in the mean flow within a wave length are so small that they affect only negligibly the dispersion relation. The absolute radian frequency ω then equals the sum of the relative radian frequency σ and the multiplication of the wave number and ambient current velocity vectors:

$$\omega = \sigma + \vec{k} \cdot \vec{u_c} \tag{3.7}$$

where $\vec{u_c}$ is the current velocity and $\vec{k}$ the wave number. which is the usual Doppler shift. For linear waves, the relative frequency is given by

$$\sigma^2 = gk \tanh(kd) \tag{3.8}$$

where, k is the wave number, g is the acceleration of gravity and d is the water depth and d is the depth. The presence of ambient currents may change the amplitude, frequency and direction of an incoming wave.

In the field of ocean wave theory, it is conventional to define a spectrum E(f) as:

$$E(f) = 2E'(f) \quad for \quad f \geq 0 \quad and \quad E(f) = 0 \quad for \quad f < 0 \tag{3.9}$$

where $E'(f)$ is the variance density spectrum (which is the Fourier transform of the auto-covariance function of the sea surface elevation, (Holthuijsen, 2007) paragraph The description of water waves through the defined variance density spectrum E(f) is called spectral description of water waves. It has been proved that the variance of the sea surface elevation is given by

$$< \eta^2 >= C(0) = \int_0^{+\infty} E(f)df \tag{3.10}$$

where C(τ) is auto-covariance function, <> represents mathematical expectation of random variable and η(t), η(t + τ) represent two random processes of sea surface elevation, τ represents the time lag. This indicates that the spectrum distributes the variance over frequencies. E(f) should therefore be interpreted as a variance density. The dimensions of E(f) are m^2/Hz if the elevation is given in m and the frequencies in Hz. The variance $< \eta^2 >$ is equal to the total energy E_{tot} of the waves per unit surface area if multiplied with a properly chosen coefficient:

$$Etot = \frac{1}{2}\rho_w g < \eta^2 > \tag{3.11}$$

The energy density as a function of frequency and direction is denoted as E(f,θ). This spectrum distributes the wave energy over frequencies and directions. As the total energy density at a frequency f is distributed over the directions θ in E(f,θ), it follows that:

$$E(f) = \int_0^{2\pi} E(f,\theta)d\theta \tag{3.12}$$

Based on the energy density spectrum, the integral wave parameters can be obtained. These parameters can be expressed in terms of the so-called n -th moment of the energy density spectrum:

$$m_n = \int_0^{\infty} f^n E(f)df \tag{3.13}$$

So, the variance of the sea surface elevation is given by $m_0 = < \eta^2 >$. Also, the significant wave height:

$$H_s = 4\sqrt{m_0} \tag{3.14}$$

and some wave periods:

$$T_{m01} = \frac{m_0}{m_1}, \quad T_{m02} = \sqrt{\frac{m_0}{m_2}}, \quad T_{m-10} = \frac{m_{-1}}{m_0} \tag{3.15}$$

3.4 Derivation of the energy balance equation

The prognostic equation of a spectral model as SWAN is the energy balance equation. According to the Eulerian approach, the energy spectrum is computed at a large number of locations simultaneously with a *local* energy balance at each of these locations. To derive the local energy balance for this approach, a cell of the geographic grid with sizes Δx and Δy in the x- and y- direction respectively, is considered. The energy balance for this cell is the bookkeeping of the energy of an arbitrary wave component (f, θ) travelling through this cell. In other words, the energy balance for this cell is the balance of the change of energy in the cell over the time interval Δt against the net import and the local generation of energy :

Change of energy in cell = net import of energy + local generation of energy

Change of energy in cell during the time interval $\Delta t =$

$=$ energy in cell at the end of interval - the energy in cell at the start of the interval

$= \left(E(f,\theta)\Delta x\Delta y + \frac{\partial E(f,\theta)}{\partial t}\Delta x\Delta y\Delta t\right) - E(f,\theta)\Delta x\Delta y$

$= \frac{\partial E(f,\theta)}{\partial t}\Delta x\Delta y\Delta t$

Net import of energy during the time interval Δt

$=$ net import of energy in the x-direction - net import of energy in the y-direction energy

$= c_{g,x}E(f,\theta)\Delta y\Delta t - \left(c_{g,x}E(f,\theta) + \frac{\partial c_{g,x}E(f,\theta)}{\partial x}\Delta x\right)\Delta y\Delta t$

$+ \; c_{g,y}E(f,\theta)\Delta x\Delta t - \left(c_{g,y}E(f,\theta) + \frac{\partial c_{g,y}E(f,\theta)}{\partial y}\Delta y\right)\Delta x\Delta t$

$= -\frac{\partial c_{g,x}E(f,\theta)}{\partial x}\Delta x\Delta y\Delta t - \frac{\partial c_{g,y}E(f,\theta)}{\partial y}\Delta x\Delta y\Delta t$

Locally generated energy

$= S(f,\theta)\Delta x\Delta y\Delta t$

with $S(f,\theta)$ representing the source term, representing all effects of generation, wave - wave interactions and dissipation per unit time per unit surface area.

In total, the energy balance for the cell $\Delta x\Delta y$ over the time interval Δt is :

$$\frac{\partial E(f,\theta)}{\partial t}\Delta x\Delta y\Delta t + \frac{\partial c_{g,x}E(f,\theta)}{\partial x}\Delta x\Delta y\Delta t + \frac{\partial c_{g,y}E(f,\theta)}{\partial y}\Delta x\Delta y\Delta t = S(f,\theta)\Delta x\Delta y\Delta t \quad (3.16)$$

where $c_{g,x} = c_g\cos\theta$ and $c_{g,y} = c_g\sin\theta$ and c_g is the propagation speed of wave energy (*group velocity*). Dividing all the terms by $\Delta x\Delta y\Delta t$ and adding again the dependence on time and horizontal space in the notation, the spectral energy balance equation for each wave component, each cell, at each moment in time, in deep water arises:

$$\frac{\partial E(f,\theta;x,y,t)}{\partial t} + \frac{\partial c_{g,x}E(f,\theta;x,y,t)}{\partial x} + \frac{\partial c_{g,y}E(f,\theta;x,y,t)}{\partial y} = S(f,\theta;x,y,t) \quad (3.17)$$

In shallow waters, the spectral energy balance is formulated in the same manner as it is for deep waters. The only differences are that (1) it involves a more complicated formulation for the propagation of the wave energy, which now needs to account for shoaling, refraction and diffraction, and (2) the number and complexity of the source terms are greater, since, in addition to the processes of wave generation by wind, quadruplet wave - wave interactions and white - capping, also triad wave - wave interactions, bottom friction and depth - induced breaking need to be represented.

In the energy balance equation for coastal waters, shoaling is accounted for by using the depth - dependent group velocity in the equation. Refraction and diffraction require an additional propagation term in the equation. The reason is that, as the energy density of an individual wave component travels through the coastal region, it changes direction. In other words, while the wave energy propagates through x, y - space is simultaneously propagates through θ space.

For the derivation of the propagating term in θ space, the directional energy distribution at each frequency in the spectrum is discreatised into directional bins, each with a width $\Delta\theta$. In the energy balance, the directional turning of the waves is presented as energy moving from one directional bin to the next as follows:

Net import of energy in θ

= (imported energy through the left - hand side of the bin) - (exported energy through the right - hand side of the bin) during the interval Δt

$$= c_\theta E(f,\theta)\Delta x\Delta y\Delta t - \left(c_\theta E(f,\theta) + \tfrac{\partial c_\theta E(f,\theta)}{\partial\theta}\Delta\theta\right)\Delta x\Delta y\Delta t$$

$$= -\tfrac{\partial c_\theta E(f,\theta)}{\partial\theta}\Delta\theta\Delta x\Delta y\Delta t$$

Adding the result to the deep - water energy balance 3.16 gives:

$$\frac{\partial E(f,\theta)}{\partial t}\Delta x\Delta y\Delta\theta\Delta t + \frac{\partial c_{g,x}E(f,\theta)}{\partial t}\Delta x\Delta y\Delta\theta\Delta t + \frac{\partial c_{g,y}E(f,\theta)}{\partial t}\Delta x\Delta y\Delta\theta\Delta t + \tag{3.18}$$

$$+\frac{\partial c_\theta E(f,\theta)}{\partial\theta}\Delta\theta\Delta x\Delta y\Delta t = S(f,\theta)\Delta x\Delta y\Delta\theta\Delta t$$

Dividing by $\Delta x\Delta y\Delta\theta\Delta t$, the Eulerian spectral energy balance equation for arbitrary depth, which applies to all wave frequencies, all directions, all locations (geographic cells) and all points in time, including the effects of directional turning (in Cartesian co-ordinates and adding the x, y, t-dependence in the absence of an ambient current), in shallow water:

$$\frac{\partial E(f,\theta;x,y,t)}{\partial t} + \frac{\partial c_{g,x}E(f,\theta;x,y,t)}{\partial x} + \frac{\partial c_{g,y}E(f,\theta;x,y,t)}{\partial y} + \frac{\partial c_\theta E(f,\theta;x,y,t)}{\partial\theta} = S(f,\theta;x,y,t) \tag{3.19}$$

where c_θ is the refraction- or diffraction-induced turning rate of the individual wave components.

Therefore, in the case that ambient currents are present, the energy density $E(f,\theta)$ is written in terms of the relative frequency $E(\sigma,\theta)$. Also, the energy balance equation needs to account also for the energy transfer between waves and currents and its effects on the propagation of the waves, which are refraction, energy bunching and frequency shifting. The latter phenomenon can be accounted for by adding a propagation term in frequency space.The derivation of this extra propagation term is essentially the same as the above derivation of the refraction term (the only difference is that direction needs to be replaced with frequency).

However, the energy transfer between waves and currents requires the addition of terms that represent the effect of work done by the current against the radiation stresses, which are associated with the momentum transport. To avoid the derivation of these complex terms, the action balance equation is considered instead of the energy balance equation. The *action density* N is the contribution of waves in a certain direction and with a certain frequency to the total wave action. The action density is a function of space and time (on a scale large compared with wave length and period) and of spectral coordinates (wave frequency and direction). In contrast to wave energy, wave action is conserved in the presence of currents (Whitham, 1974 ; Svendsen, 2006).

The wave action, N, is closely related to the wave energy, E, according to the following equation:

$$N(\sigma,\theta) = \frac{E(\sigma,\theta)}{\sigma} \tag{3.20}$$

The action balance equation, with frequency-shifting included, in Cartesian co-ordinates is given by (Booij et al.1999 & Holthuijsen 2007):

$$\frac{\partial N(\sigma,\theta;x,y,t)}{\partial t} + \frac{\partial c_x N(\sigma,\theta;x,y,t)}{\partial x} + \frac{\partial c_y N(\sigma,\theta;x,y,t)}{\partial y} + \\ + \frac{\partial c_\theta N(\sigma,\theta;x,y,t)}{\partial \theta} + \frac{\partial c_\sigma N(\sigma,\theta;x,y,t)}{\partial \sigma} = \frac{S_{tot}}{\sigma} \tag{3.21}$$

Using the proper expressions for the propagation speeds c_g and c_θ and c_σ in the action balance equation, which are derived from the linear theory (Holthuijsen, 2007 ; Whitham, 1974; Mei, 1983) the effects of wave propagation (shoaling, refraction and frequency shifting ; diffraction is neglected here) are accounted for:

$$\frac{D\vec{x}}{Dt} = (c_x, c_y) = \vec{c_g} + \vec{u} = \frac{1}{2}\left(1 + \frac{2|\vec{k}|d}{\sinh(2|\vec{k}|d)}\right)\frac{\sigma\vec{k}}{|\vec{k}|^2} + \vec{u} \tag{3.22}$$

$$\frac{D\theta}{Dt} = c_\theta = -\frac{1}{k}\left(\frac{\partial\sigma}{\partial d}\frac{\partial d}{\partial m} + \vec{k}\cdot\frac{\partial\vec{u}}{\partial m}\right) \tag{3.23}$$

$$\frac{D\sigma}{Dt} = c_\sigma = \frac{\partial\sigma}{\partial d}\left(\frac{\partial d}{\partial t} + u\frac{\partial d}{\partial s}\right) - c_g k\frac{\partial u_n}{\partial n} \tag{3.24}$$

where,c_x, c_y are the propagation velocities of wave energy in spatial x -, y -space, c_σ and c_θ are the propagation velocities in spectral space σ -, θ -space, d is water depth, u_n is the component of the current velocity in the wave direction (normal to the crest) and s is the coordinate in the current direction, and s m is a co-ordinate perpendicular to s.

The right-hand side of the equation contains source terms, i.e. terms which model the generation and dissipation of wave energy. In contrast with the propagation terms most of the source terms are empirical in nature and contain empirical "constants". SWAN has default values for almost all of these constants; these values are mostly based on literature, and have been obtained by studying laboratory experiments or field observations. Due to the empirical nature of parts of the model a verification is needed for every new application of the model. The chapter on usage of numerical models also describes how to calibrate and validate a simulation model.

$$S_{tot} = S_{in}(\sigma,\theta_w) + S_{nl4}(\sigma,\theta_w) + S_{nl3}(\sigma,\theta_w) + S_{wcap}(\sigma,\theta_w) + S_{br}(\sigma,\theta_w) + S_{bot}(\sigma,\theta_w) \tag{3.25}$$

The total sum of the source and sink terms are divided into the wind source term S_in, non-linear three- and four-waves interaction terms S_{nl3} and S_{nl4} respectively, and dissipation terms. The dissipation terms include the dissipation due to depth-induced breaking S_{br}, dissipation due to bottom friction S_{bot} and dissipation due to white capping S_{wcap}. For more details about the modeled processes and the numerical methods used in SWAN, the reader is refered to (Holthuijsen, 2007) and (Wave, User manual).

For a full wave-current interaction, the currents from Delft3D-FLOW are used in Delft3D-WAVE (current refraction). The procedure is known as the *coupling* of the two models. The interaction between waves and currents is implemented by running the wave model every N flow timesteps. The wave module must run before the flow module. A communication file is created that contains the results of the wave simulation (rms wave height, peak period, wave direction, mass fluxes etc). The flow module can read then the wave results and include them in the flow simulation. The reason that the wave model is called more than once is that the computed wave model must be updated in order to account for the changed water depths and flow properties. At each call to the wave module, the latest bed and water elevations and current velocities are transferred from the flow module.

Chapter 4

Test case and model setup

In this study, the Delft3d model is used to simulate the Meltemi event and forecast its effects, as this was experienced in July of 2003 at Gouves beach. Besides deriving information about the wave climate and the sediment transport under the influence of the Meltemi event, the forecasted results are compared with the field measurements of (Poulos *et. al.*, 2012, Poulos *et. al.*, 2013). The eventual quantitative agreement is the outcome of the fine tuning and calibration of the Delft3D modules, for a collaborative and coupled performance through artificial boundaries and appropriate boundary conditions, nested grids and a suitable representation of the solution for the exterior wave problem.

The study site, Gouves beach, is situated at the north coastline of Crete, approximately 28 km to the east of the city of Heraklion. It is an open, sandy beach zone developed in front of a gently sloping ($< 2.5\%$) Holocene alluvial plain and has a length of 2.5 km, width up to 20 m and a gently sloping (1% for 0-15 m and 2-3% for 15-50 m of water depth) nearshore bathymetry (Poulos *et. al.*, 2012, Poulos *et. al.*, 2013). The physiographic characteristics of the beach are listed in table 4.1. The tidal range is small (< 10 cm) and the tide at Heraklion harbor is characterised by (Tsimplis,1994) as mixed, mainly diurnal, according to the Form Factor introduced by (Pugh, 1996). It is exposed to northwesterly, northerly, and, partially easterly winds and experiences a rather intense wave regime, with the dominant wind - generated waves approaching from the north and northwest.

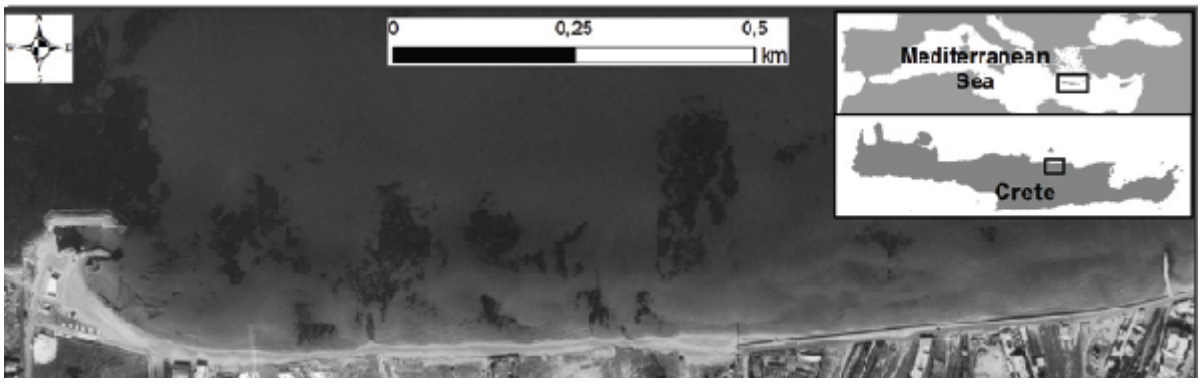

Figure 4.1: The area of interest

Numerical simulations were carried out by means of a coupling between the Delft3D - FLOW model and the Delft3D - WAVE model. The coupling time step was set to 50 min. The two

Beach Area	
Length	2.5km
Width	1 - 12m
Material	Sand
Underwater Slope	
0 - 15 m	1%
15 - 50 m	3%
Alluvial Plane	
Width	$\approx$ 750 m
Slope	$<$ 2.5%
Catchment Area	
Gournianos	Gouvianos
32.95 km	18.35 km

Table 4.1: Physiographic characteristics of the study area

models exchange information through a communication file (fig. 4.2). The wave model runs at first, then Delft3D - FLOW model reads the results of the wave simulation (significant wave height, wave period, wave direction, mass fluxes etc.) and includes them in the flow calculations. Then, the results from the flow simulation (updated bathymetry, water level and flow velocities) are passed back to the wave model through the communication file.

The wave model runs in a stationary mode whereas the flow equations are solved with a computational time step of 12s, which fulfills the Courant − Friedrichs Lewy (CFL) criterion for wave propagation:

$$CFL_{wave} = 2\Delta t\sqrt{gH}\sqrt{\frac{1}{\Delta x^2} + \frac{1}{\Delta y^2}} < 1 \tag{4.1}$$

where Δt is the time step, g is the acceleration of gravity, H is the total water depth and Δx,Δy are the smallest grid spaces in x - and y -direction of the physical space.

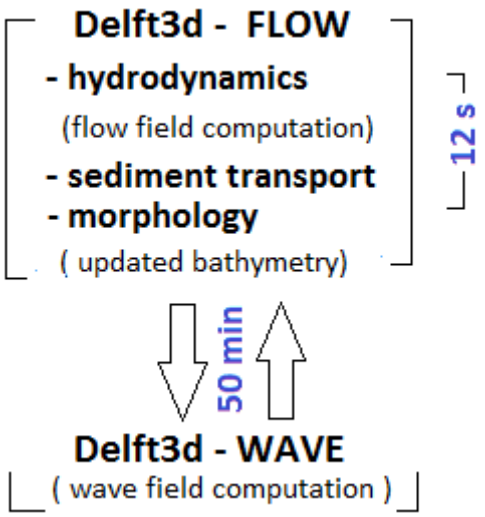

Figure 4.2: Scheme of a morphodynamic simulation

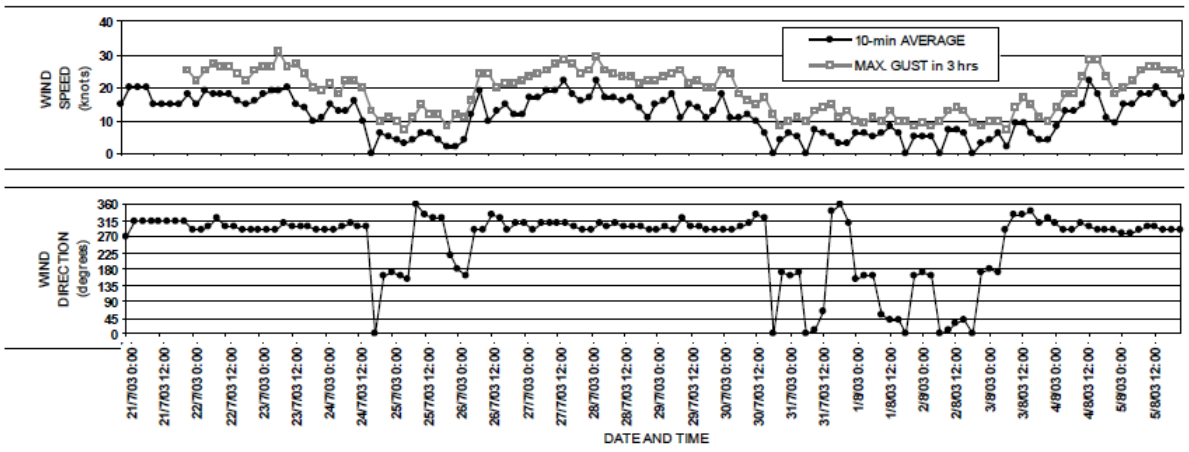

Figure 4.3: Wind speed (mean values and gusts) and direction at the Heraklion Airport weather station, for the period 21st July to 5th August 2003

Station	**Latidude**	**Longitude**	**Distance from the shoreline (m)**	**Depth(m)**
G1	$35^o20.157'$	$25^o17.294'$	75	2.60
G2	$35^o20.196'$	$25^o17.306'$	122	3.95
G3	$35^o20.290'$	$25^o17.290'$	232	5.62

Table 4.2: Geographic locations and deployment depths of the recorders, (Poulos *et. al.*, 2012, Poulos *et. al.*, 2013).

As long as the Meltemi conditions are stronger at the end of July, a 7 - day simulation was performed, from 24^{th} until 30^{th} of that month. According to data collected from Heraklion airport weather station the study area experienced wind speeds in July 2003, the maximum values of which are characterized as *strong* Etesian conditions (Carapiperis, 1968). The wind speeds and directions are given as a timeseries in the model. The bathymetry used for the flow and wave computations is based on the sample data that derived during the study of (Poulos *et. al.*, 2012, Poulos *et. al.*, 2013). The bathymetry files were constructed after interpolation of these data into the computational grids.

Additionally, three observation points were used to monitor the time-dependent behaviour of the computed quantities as a function of time at specific locations. The observation points were located at cell center, i.e. at water level points on the flow grid. Their position is identical to the location in which three Autonomous Benthic Recorders were located at increasing distances from the shoreline (75m, 122m, and 232m respectively), in order to measure suspended sediment concentrations, current speed and direction and wave characteristics during the study of (Poulos *et. al.*, 2012, Poulos *et. al.*, 2013). In table 4.2 , the specific geographic locations of the recorders are shown.

Artificial boundaries and exterior wave problem

For the calculations we constructed three computational domains that are presented in figure 4.4.

The flow grid was built based on the available bathymetry, with a size of 1465 m and 1500 m in the cross-shore and long-shore direction, respectively. The resolution of the flow grid is $\Delta x = \Delta y = 12.5$m and the depth of closure is approximately 18m.

For the flow computations, the vertical space was discretized in 12 σ - layers with a thickness of 2.0%, 3.2%, 5.0%, 7.9%, 12.4%, 19.6%, 19.6%, 12.4%, 7.9%, 5.0%, 3.2%, 1.8%, of the total water depth, starting from the surface towards the bottom.

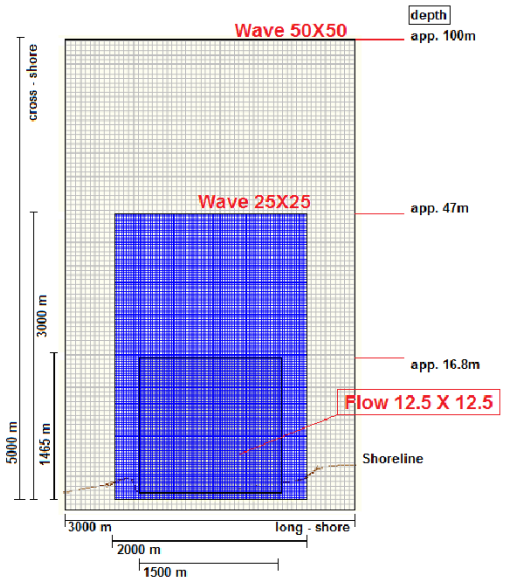

Figure 4.4: Scheme of the hierarchical (nested) grids

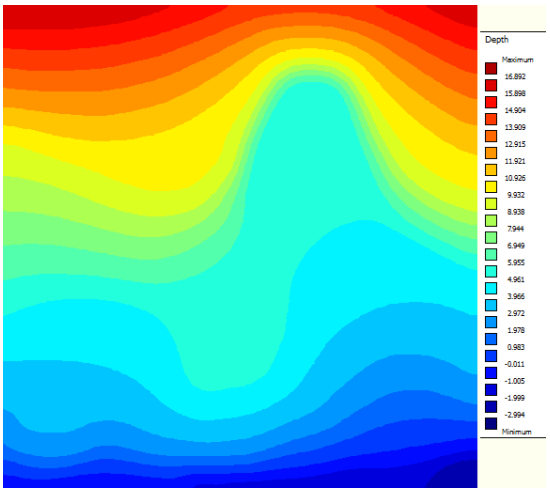

Figure 4.5: Bathymetry used for the flow computations

The computational flow domain is limited by 4 boundaries: One closed boundary (South) and three open boundaries (North, West and East). The closed boundary represents the coastline. The other three, the open boundaries, are artificial water -water boundaries. They are introduced to obtain a limited computational area and so to reduce the computational effort. They are situated as far as possible from the area of interest in order to avoid any disturbances to propagate into it. At the north, a uniform water level boundary is imposed as a timeseries, with a sinusoidal profile with range of $\approx 10cm$ (Tsimplis, 1994). The lateral open boundaries are gradient - type (Neumann) boundaries equal to zero, allowing the wind - induced setup to freely develop at the lateral boundaries and thus, a better solution to be obtained (Roelvink *et. al.*, 2004). Furthermore, for the transport boundary conditions we have set Neumann boundary conditions at the open inflow boundaries. This choice means that at all open inflow boundaries, the flow should enter carrying all sediment at its equilibrium concentration profiles. Thus, by setting the sediment concentrations at the boundary equal to those just inside the model domain, we can avoid erosion or accretion phenomena near the boundaries. Additionally, no boundary condition is prescribed at the outflow boundaries, meaning that the dispersive transport of sediment at the outflow boundary is neglected compared to the advective transport.

For the dependent variables, uniform initial conditions are chosen. Particularly, a zero value was set for the water level and a value of 0.015 kg/m^3 for the sediment concentration.

For the calculation of the wave field we constructed two increasingly resolved nested wave grids. The coarser grid has a resolution of 50m in both directions and covers an area of 5000m and 3000m in the cross-shore and long-shore direction, respectively. The reason that we constructed these two hierarchical grids is to achieve a smooth transition from the offshore wave conditions to that close to the shoreline.

We prescribe only the incident wave conditions at the boundaries of the coarser grid while the nested grid obtains its boundary conditions from the coarser grid. On the coarse grid we defined three open boundaries (North, East, West) with the same boundary conditions prescribed. For the derivation of these conditions we used the deepwater hindcasts from (Poulos *et. al.*, 2012, Poulos *et. al.*, 2013) for the significant wave height (Hs) and the peak period (Tp) in the three principal directions of generation N, NW and W, that cover the range of wind speeds (U) experienced during the study period.

They are summarized in table 4.3. For their calculation the deepwater wave forecasting equations were used (Jonswap model, Hasselmann *et. al.*1973), which are presented in table 4.4.

U(m/s)	**Hs(m)**			**Tp(s)**		
	N	**NW**	**W**	**N**	**NW**	**W**
1	0.013	0.013	0.013	0.589	0.589	0.589
2	0.069	0.069	0.069	1.382	1.382	1.382
3	0.187	0.187	0.187	2.276	2.276	2.276
4	0.379	0.379	0.327	3.242	3.242	2.940
5	0.656	0.656	0.430	4.266	4.266	3.222
6	1.027	1.027	0.538	5.339	5.339	3.472
7	1.484	1.501	0.651	6.409	6.454	3.698
8	1.749	2.084	0.767	6.770	7.606	3.906
9	2.022	2.785	0.886	7.105	8.791	4.099
10	2.302	3.358	1.009	7.418	9.541	4.280
11	2.588	3.775	1.134	7.714	9.921	4.451
12	2.881	4.202	1.263	7.994	10.28	4.613
13	3.179	4.637	1.393	8.261	10.62	4.767
14	3.482	5.079	1.526	8.516	10.95	4.914

Table 4.3: Deepwater hindcasts used for the offshore wave conditions

Note that the coarser grid is extended to about 100m depth contour, assuming a linear increasing depth after 1465m cross - shore, in order to cover the approximate depth of the 90m in which the hindcasted waves start shoaling (Komar, 1998).

Deepwater Wave Forecasting Equations
Hs(m), Tp(s), U(m/s), F(m), t(s) g=9.8 m/s^2
Fetch Limited (F, U)
$Hs = 5.112 \times 10^{-4} U F^{1/2}$ $Tp = 6.238 \times 10^{-2} (UF)^{1/3}$ $t = 3.215 \times 10^{1} \left(\frac{F^2}{U}\right)^{1/3}$
Fully Developed
$Hs = 2.482 \times 10^{-2} U^2$ $Tp = 8.3 \times 10^{-1} U$ $t = 7.296 \times 10^{3} U$

Table 4.4: Deepwater wave forecasting equations

The finer wave grid has a resolution of 25m in both directions. It is larger than the flow grid in order to reduce or, even better, avoid possible boundary disturbances of the wave model reaching the flow domain.

The superimposed effect of currents and waves was taken into account by means of the interaction model of (Grant *et. al.*, 1979). Turbulence effects were computed by means of the $k-\epsilon$ model. Horizontal background eddy viscosity and diffusivity were set equal to 1 m^2/s. For the sediment transport and morphodynamic computation, the default transport formula of (Van Rijn, 1993) is selected. Sediment was assumed to be sandy with a D_{10}, D_{50} and D_{90} respectively equal to $150\mu m$, $200\mu m$ and $300\mu m$, and a sediment density equal to 2650 kg/m^3. The dry bed density was set equal to $1600 kg/m^3$. The acceleration due to gravity is $g = 9.807 m/s^2$, the water density is $1025.97 kg/m^3$ and the air density assumed 1 kg/m^3.

Chapter 5

Results and Discussion

5.1 Significant wave height

The following figures show the contours of the magnitude along with the direction of the significant wave height (Hs), on selected times of the simulation.

The simulation outputs related to the significant wave height (Hs) and direction show that on 26th of July; 12:00, i.e. before the peak of the event, the coastal area of Gouves presents wave heights approximately 0.5m in WNW direction while the wind speed is 5.5 m/s (WNW)(figure 5.1).

As the waves reach the shore, refraction due to shoaling is present and the wave crests tent to be parallel to the shoreline.

One can observe that the significant wave height increases as the wind velocities increases (figures 5.2, 5.3, 5.4). Before the peak of the storm, the significant wave height has values in the range of 1m -1.7m while the wind velocity reaches the value of 9.18 m/s. Particularly, on the 27th of July (11:20) the Hs reaches 2 - 2.5 m offshore while nearshore the wave height is 1.7m (figure 5.5).

At the peak of the storm, the significant wave height can reach the 4m in some areas offshore, whereas, in the area of interest its values are in the range of 1.5m to 2.5m (U=11.1 m/s, NW) (figures 5.6, 5.7, 5.8).

This profile (figures 5.9, 5.10) is repeated on the 28th of July (10:40) when the second peak of the wind speed occurs (U=11 m/s, NW) (figures 5.11).

After the peak of the storm, the Hs is reduced until 29th of July, (5.11 - 5.15) when it starts to slightly increase again reaching the value of 0.9m in the area of interest (U 9m/s, W) (figures 5.16 - 5.18).

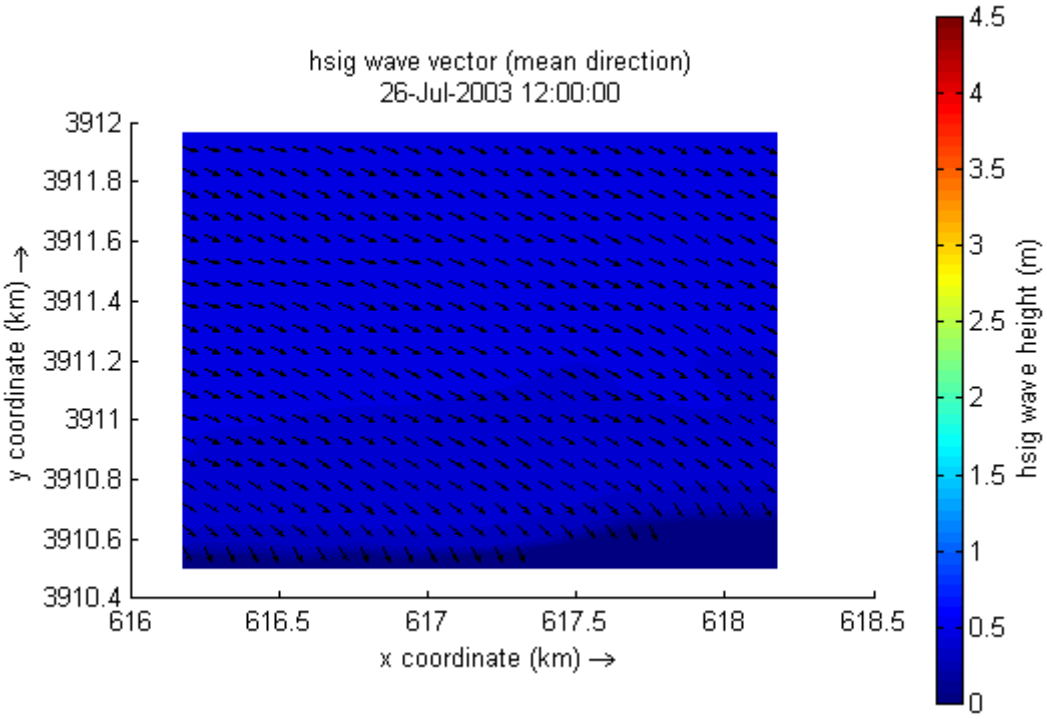

Figure 5.1: Before the peak of the storm

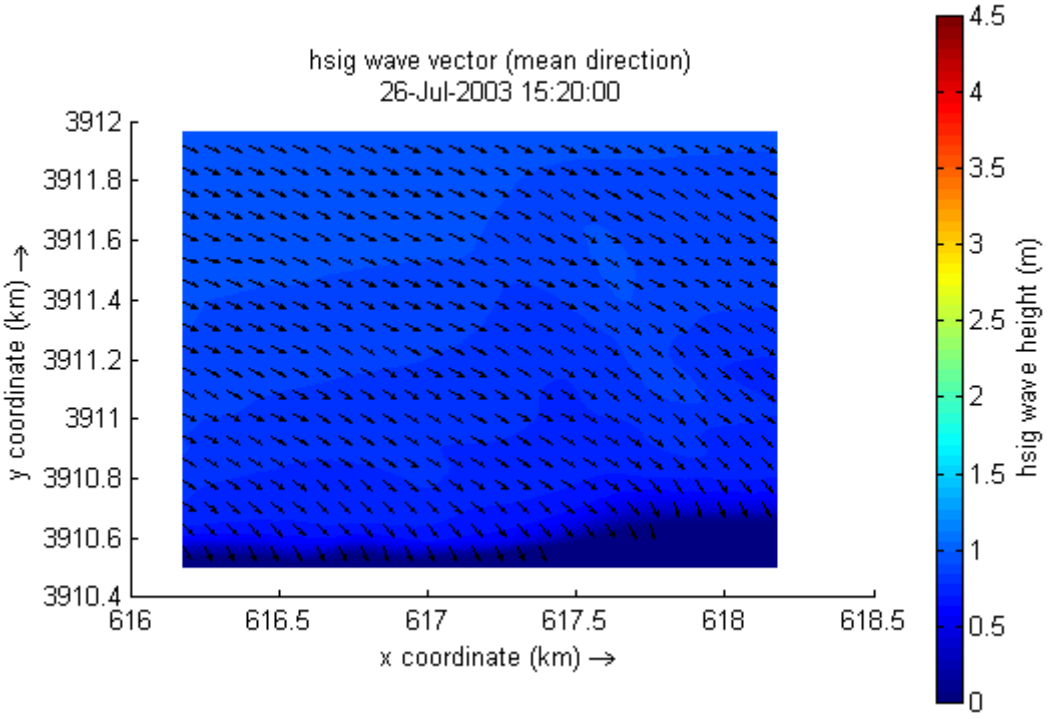

Figure 5.2: Before the peak of the storm

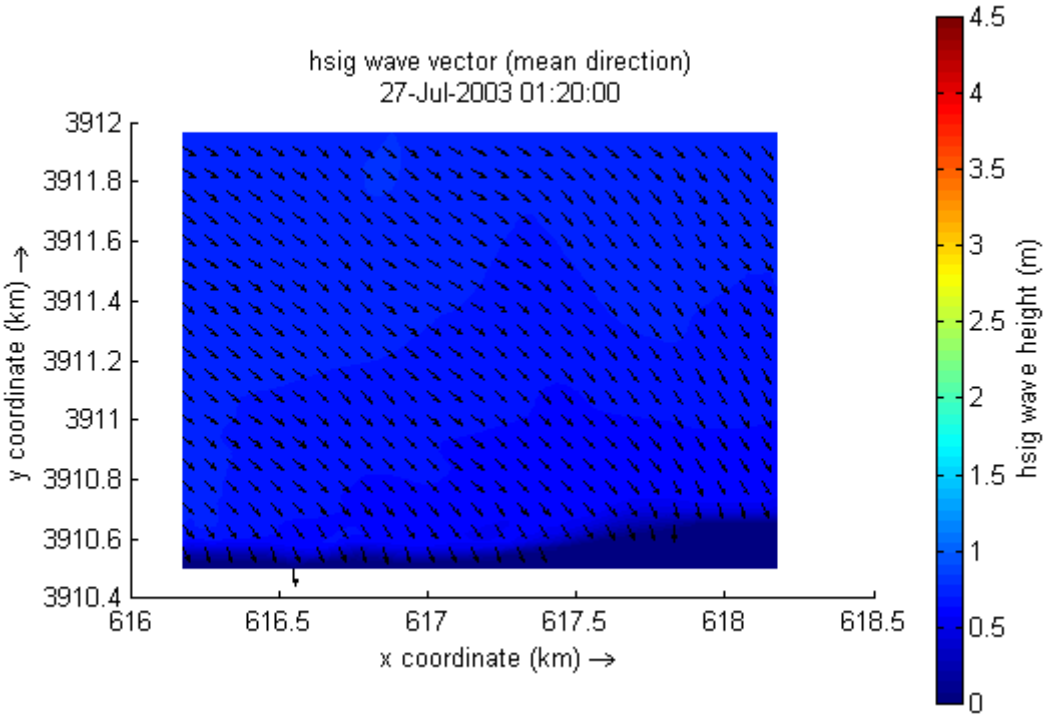

Figure 5.3: Before the peak of the storm

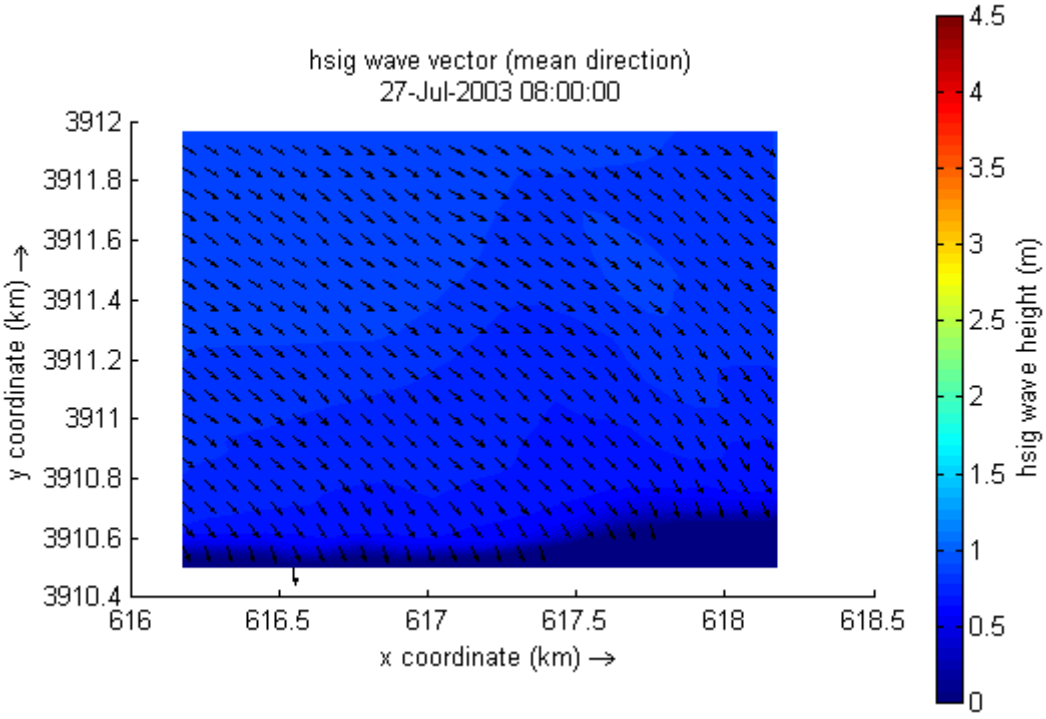

Figure 5.4: Before the peak of the storm

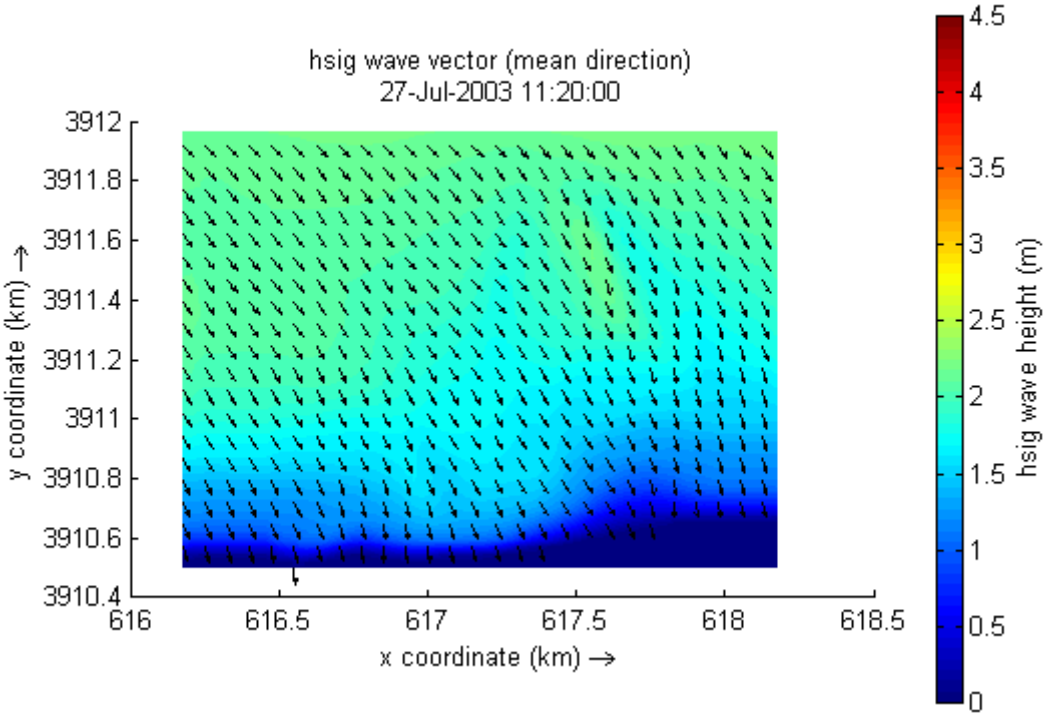

Figure 5.5: Before the peak of the storm

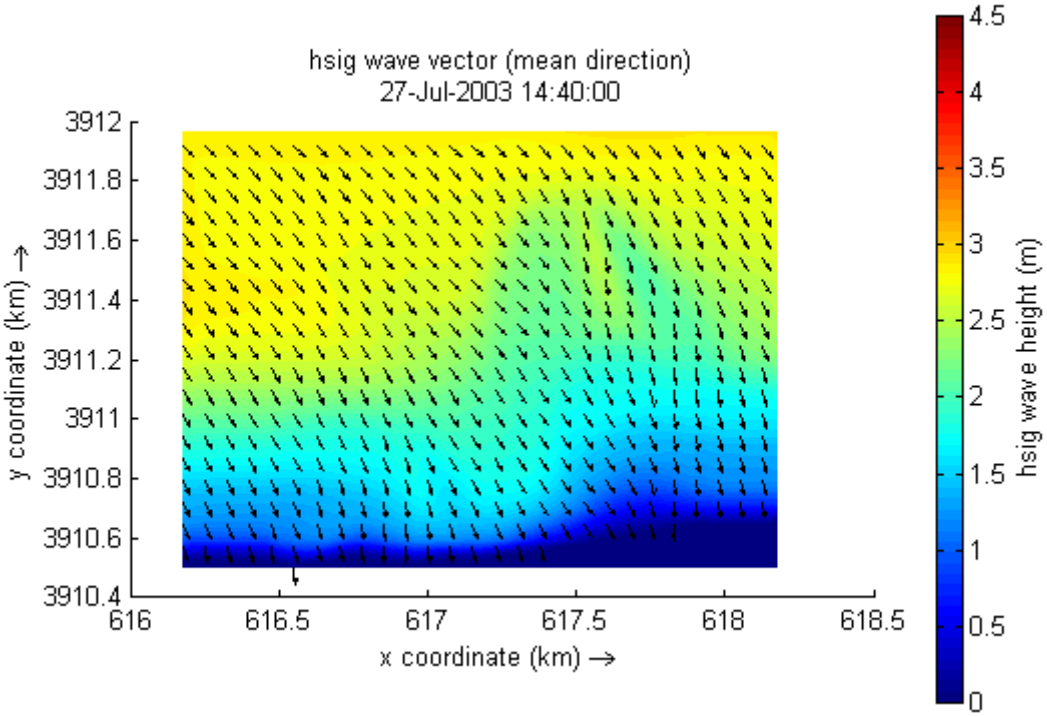

Figure 5.6: During the peak of the storm

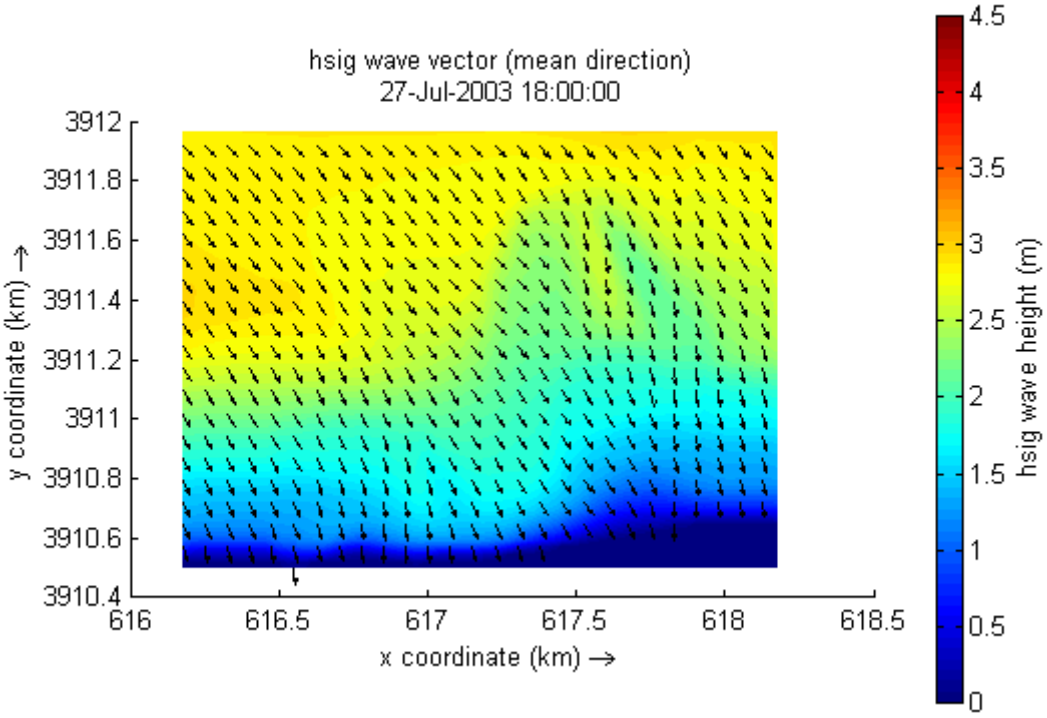

Figure 5.7: During the peak of the storm

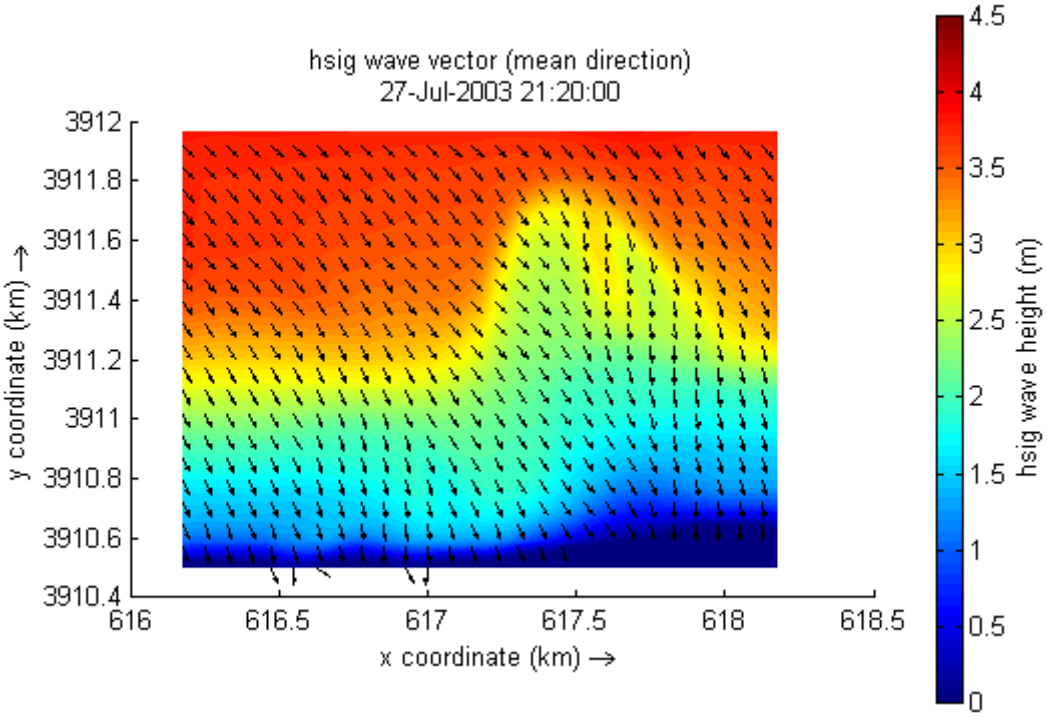

Figure 5.8: During the peak of the storm

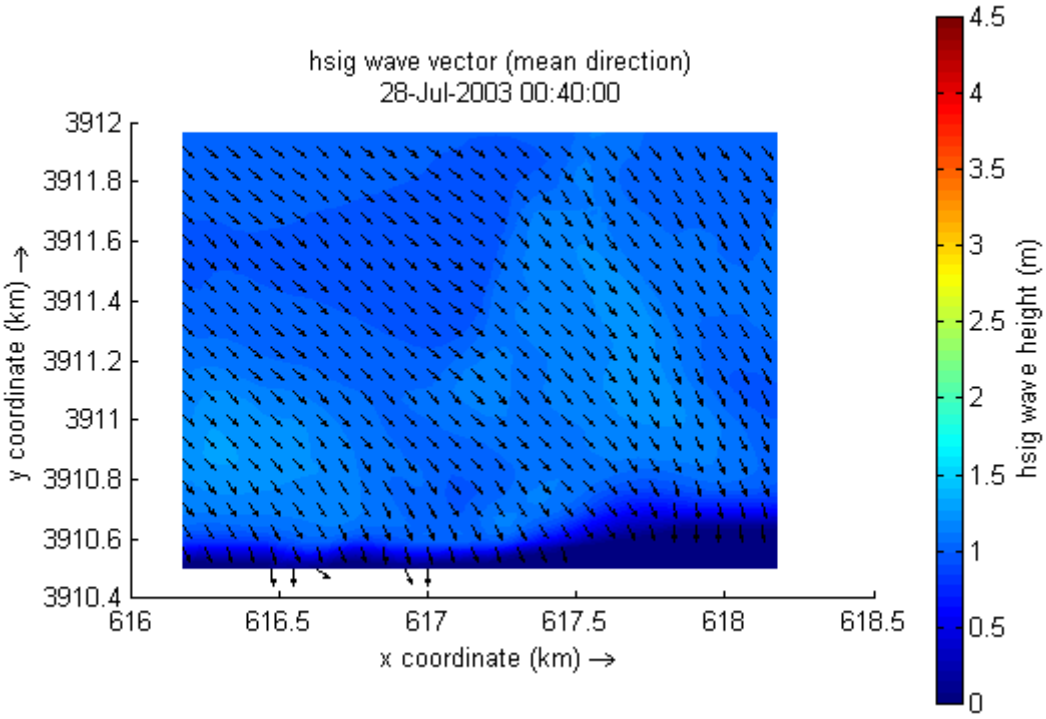

Figure 5.9: During the peak of the storm

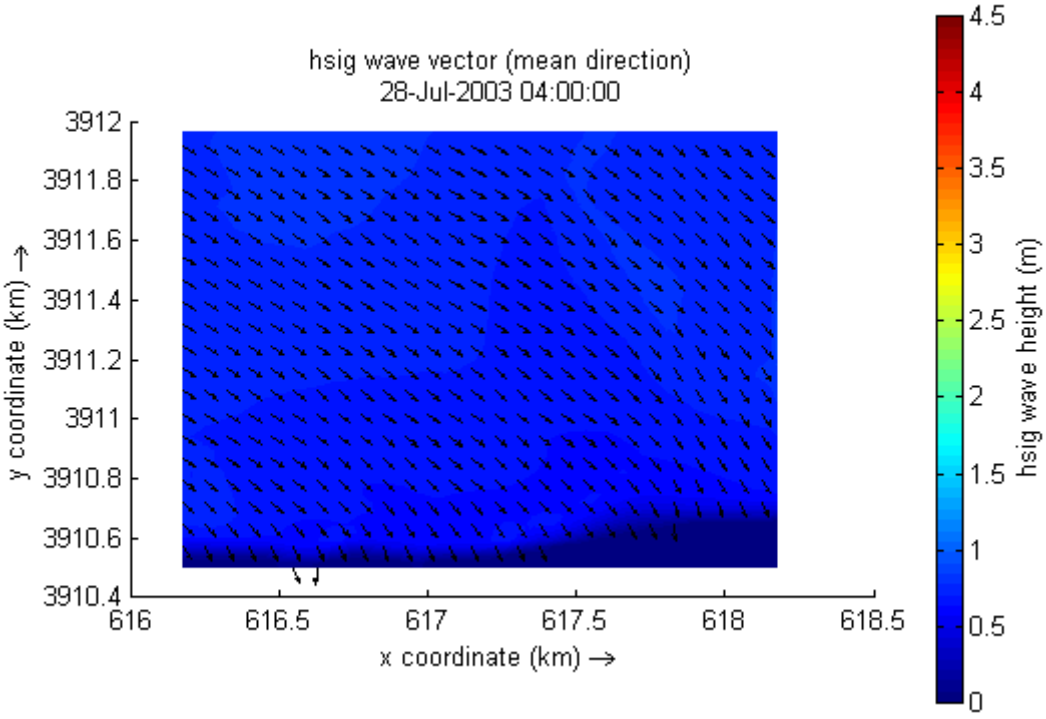

Figure 5.10: During the peak of the storm

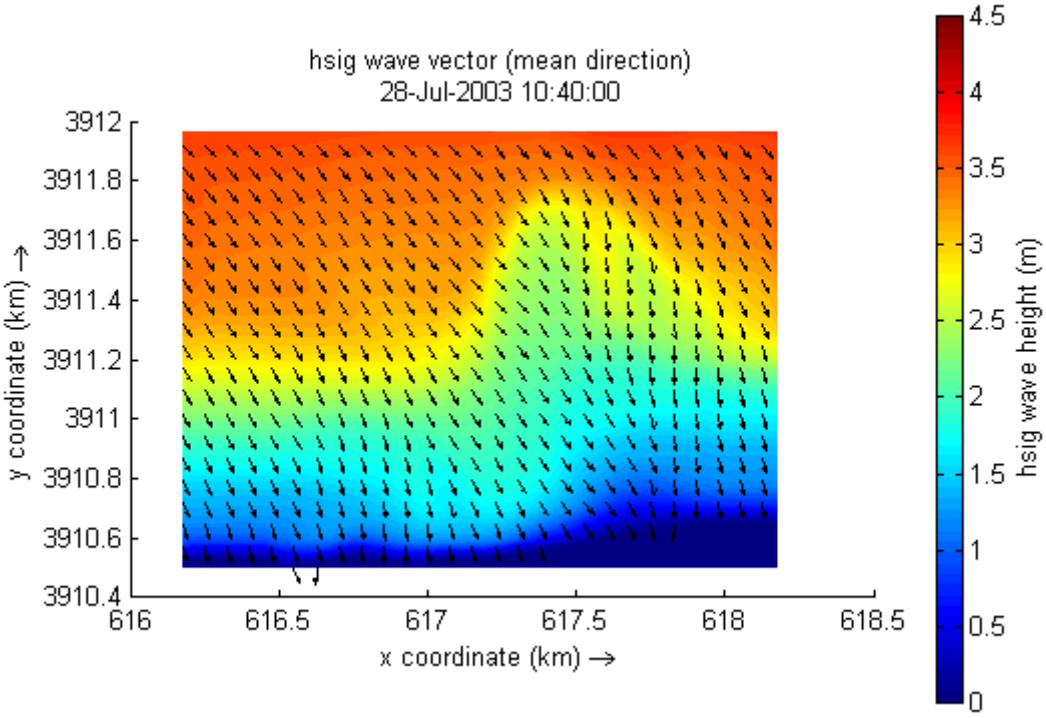

Figure 5.11: During the peak of the storm

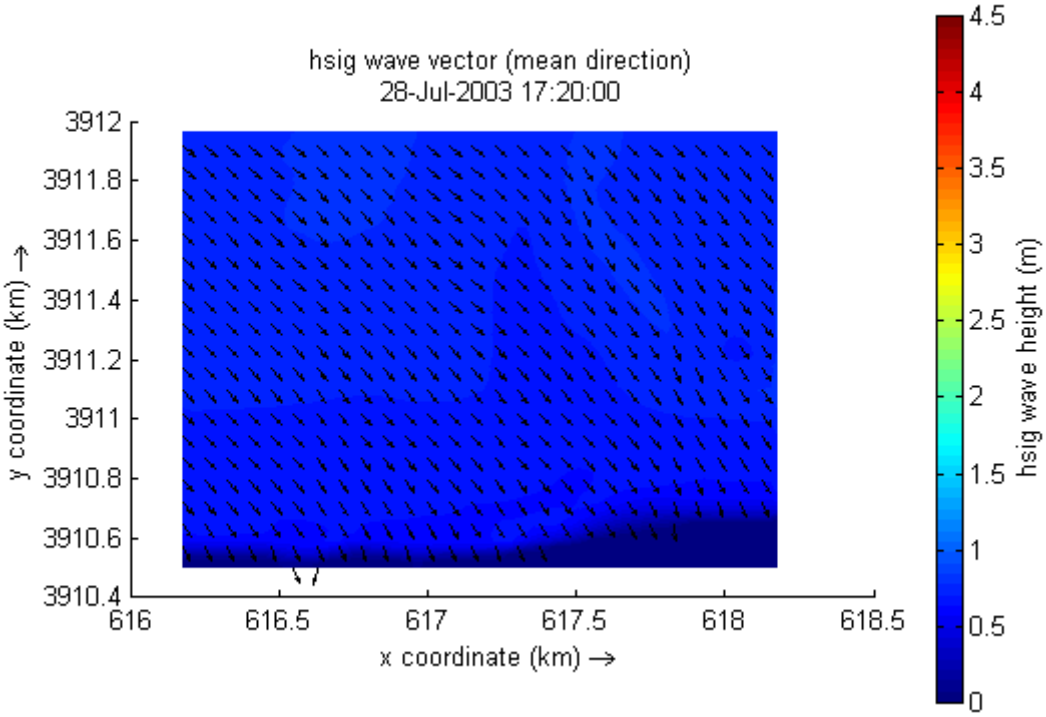

Figure 5.12: After the peak of the storm

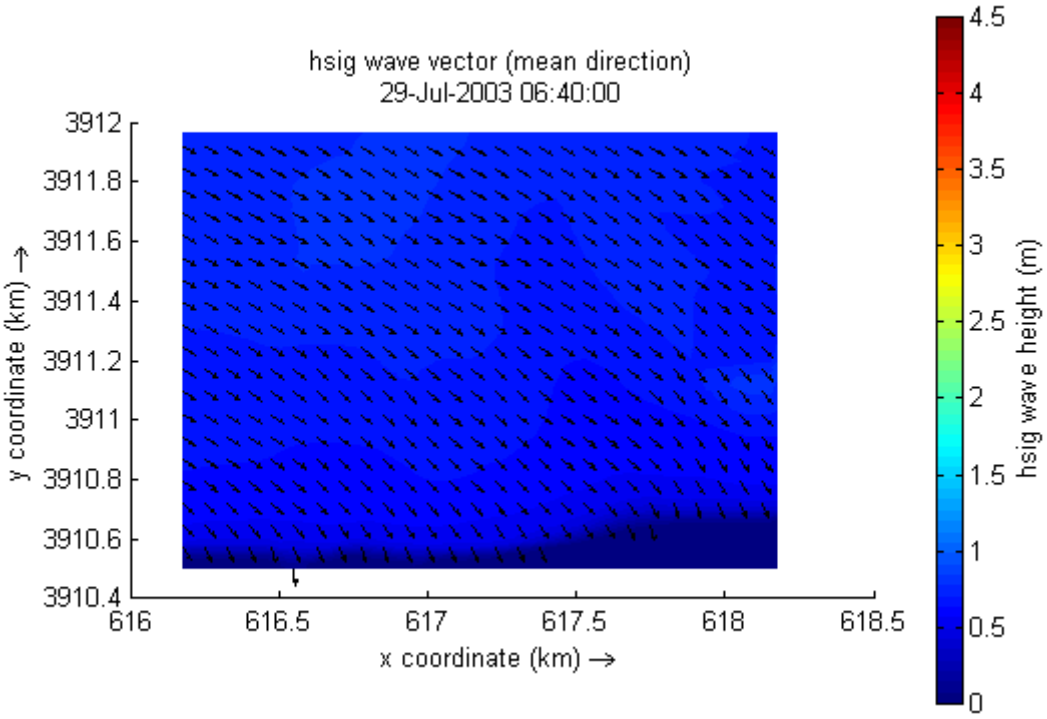

Figure 5.13: After the peak of the storm

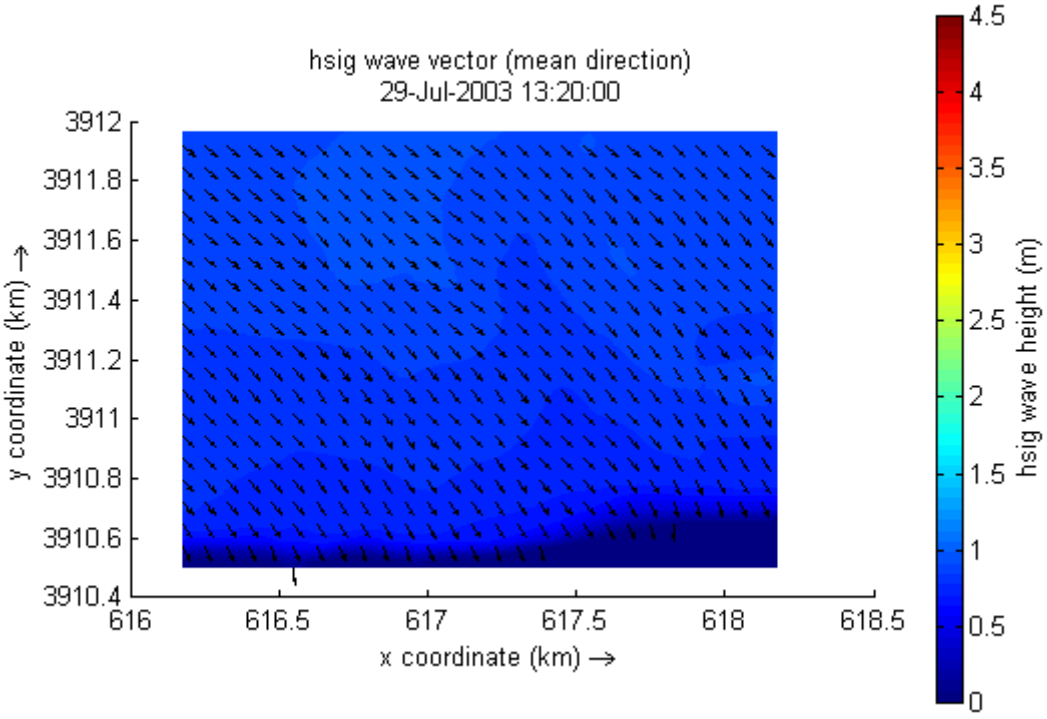

Figure 5.14: After the peak of the storm

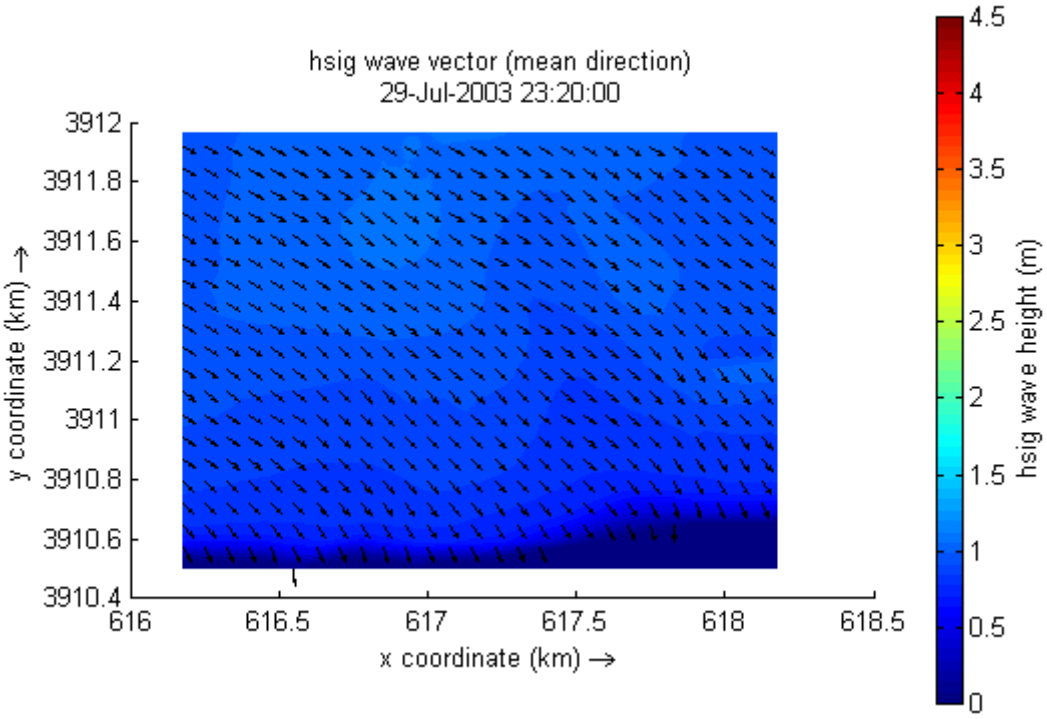

Figure 5.15: After the peak of the storm

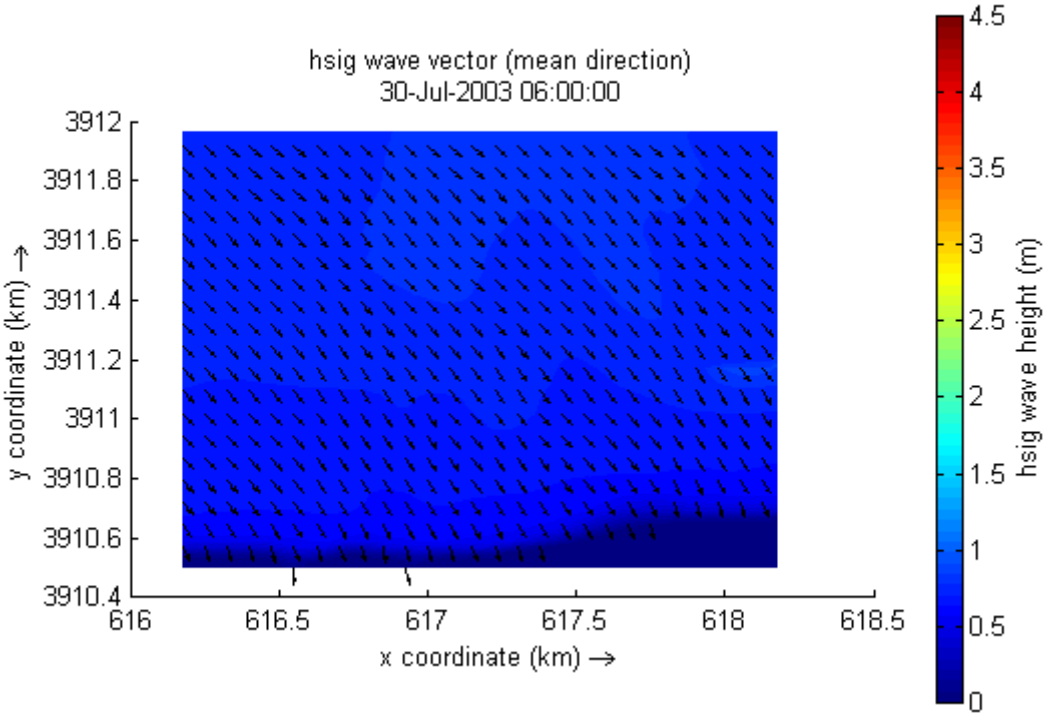

Figure 5.16: After the peak of the storm

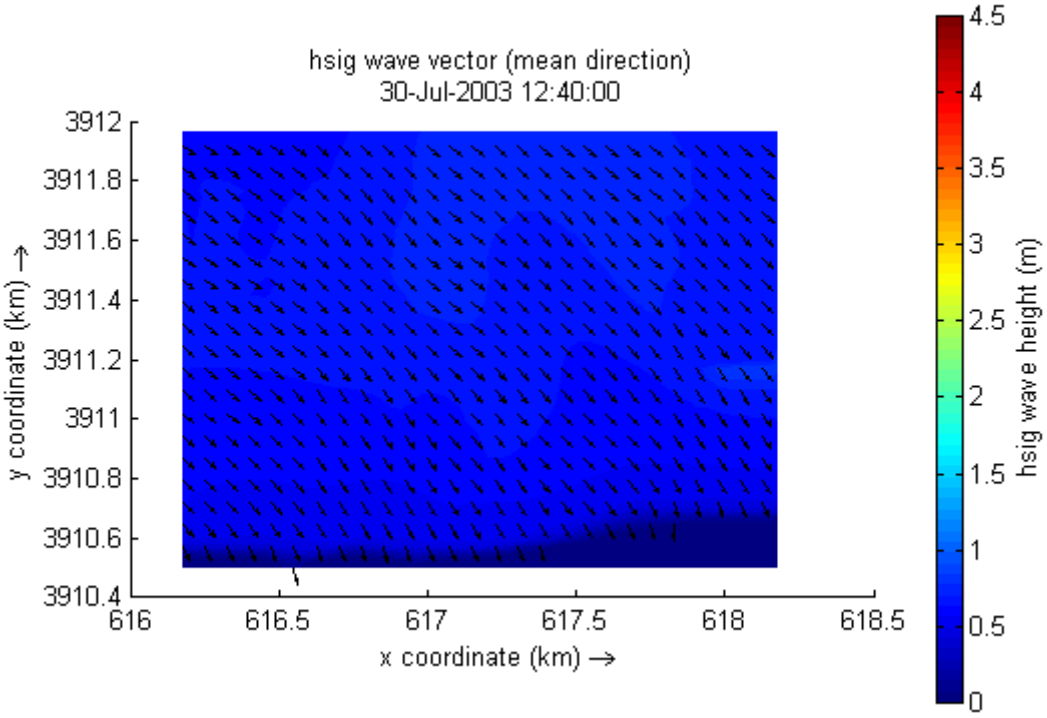

Figure 5.17: After the peak of the storm

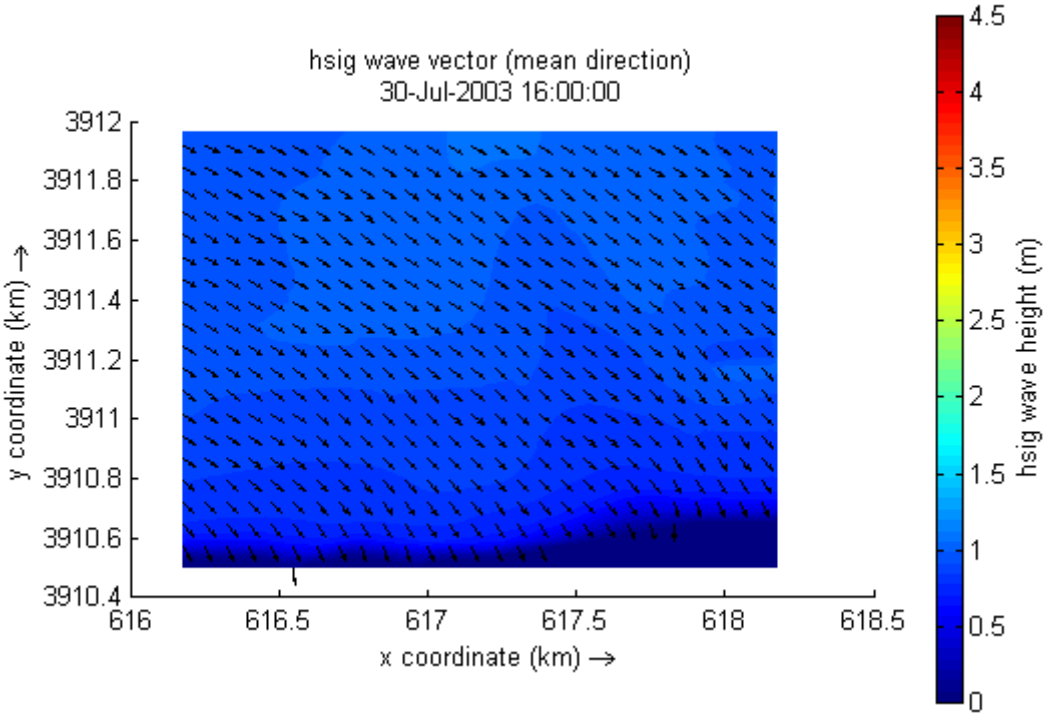

Figure 5.18: After the peak of the storm

5.2 Currents

As we already mentioned, currents in the sea play a fundamental role in the sediment transport phenomenon, as they can stir up and transport sediments. Hence, the sediment transport largely follows the current direction.

The following figures illustrate the current directions at selected times during the study period together with the associated current velocities. One can observe that the current velocity increases and decreases relative to the development of the Meltemi event. Generally, the current direction is from West to East, parallel to the shoreline.

The simulation outputs related to the current magnitude and direction show that before the peak of the event, the coastal area of Gouves presents currents with a magnitude of 0.1 m/s (figure 5.19).

As the Meltemi event develops, the current velocity reaches the value of 0.2 m/s offshore and 0.4 m/s nearshore (figures 5.20, 5.21, 5.22). On the 27th of July (11:20), just before the wind velocity to reach 11 m/s, one can observe that currents begin to feel the bottom and reach 0.5 m/s mainly nearshore (figure 5.23).

During the peak of the storm, currents can exceed the value of 0.9 m/s in some areas (figures 5.24, 5.25, 5.26, 5.27, 5.28, 5.29).

After the peak of the storm, the current velocity returns to the averaged value of 0.2 m/s in the entire area for the rest of the event (figures 5.30, 5.31, 5.32, 5.33, 5.34, 5.35, 5.36).

Furthermore, rip currents are appeared across the shoreline because of the breaking process of waves that push water towards the land.

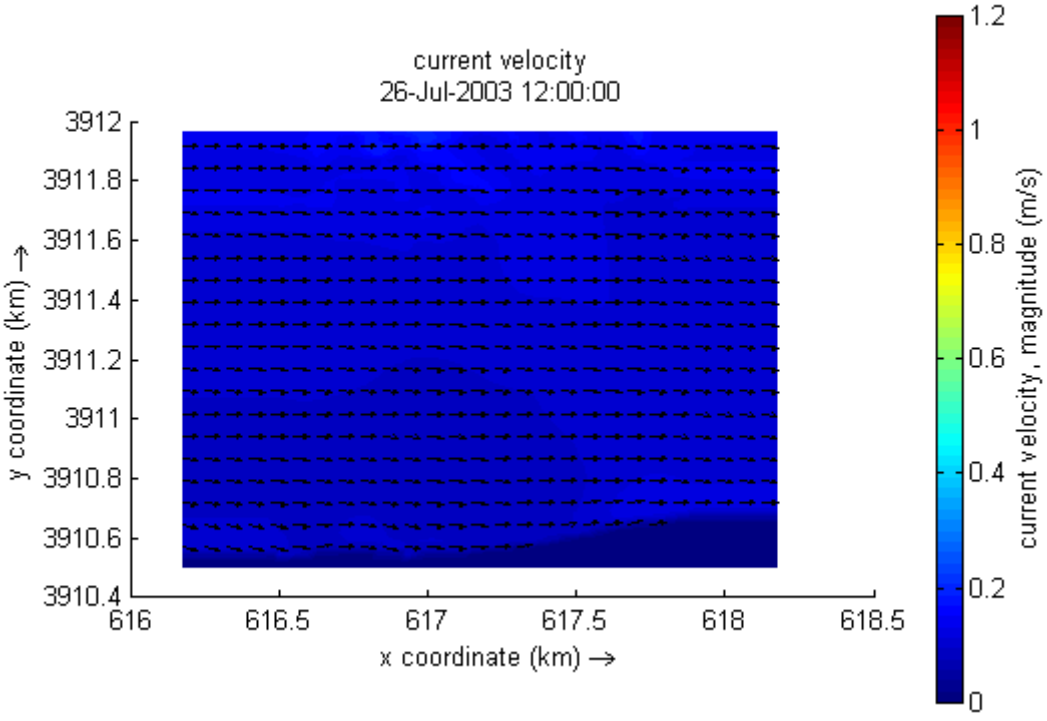

Figure 5.19: Before the peak of the storm

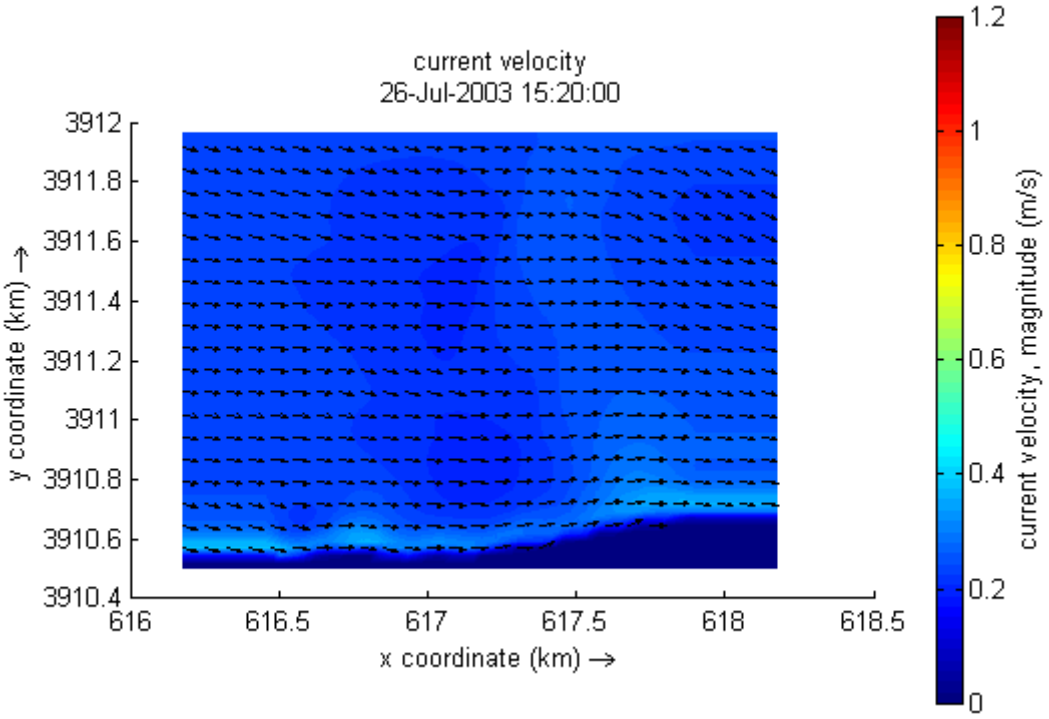

Figure 5.20: Before the peak of the storm

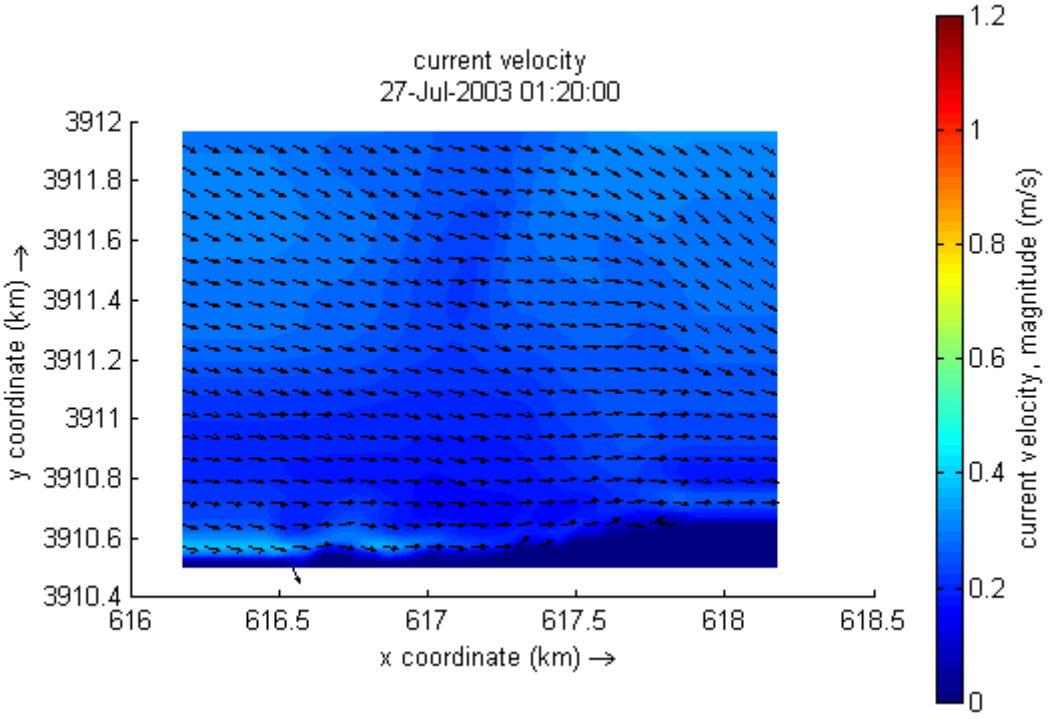

Figure 5.21: Before the peak of the storm

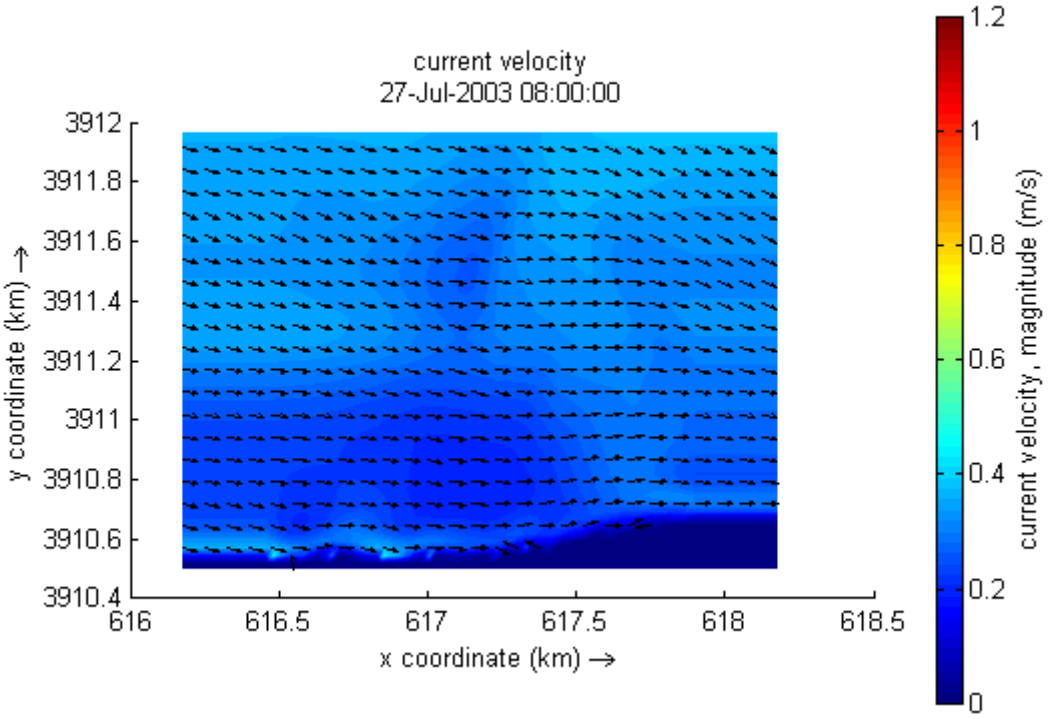

Figure 5.22: Before the peak of the storm

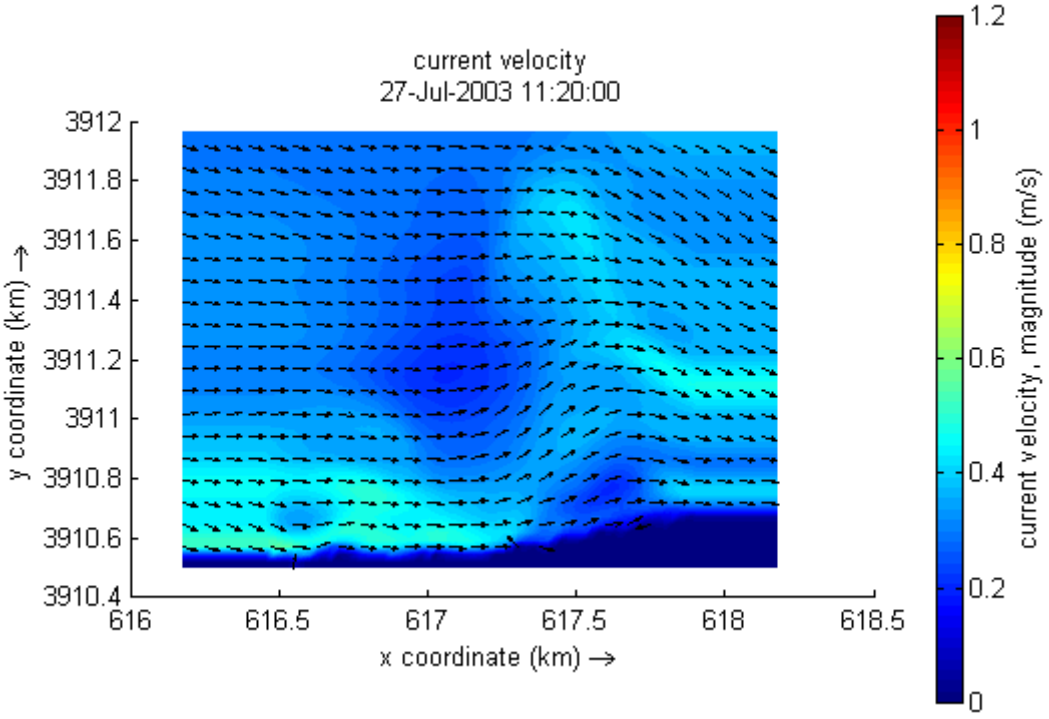

Figure 5.23: Before the peak of the storm

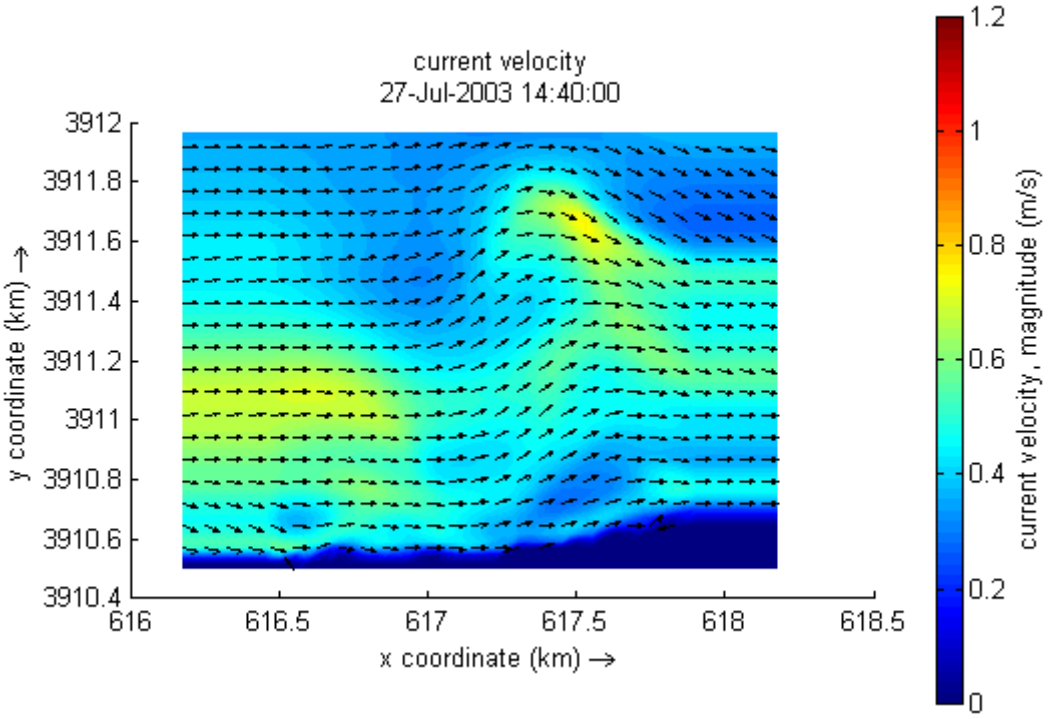

Figure 5.24: During the peak of the storm

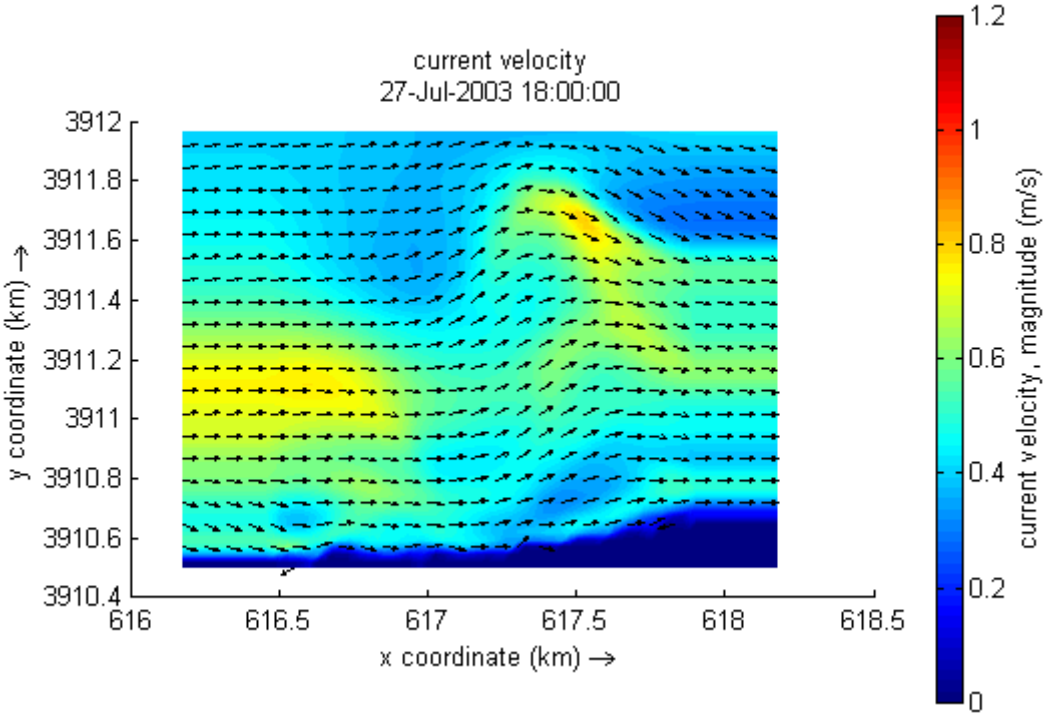

Figure 5.25: During the peak of the storm

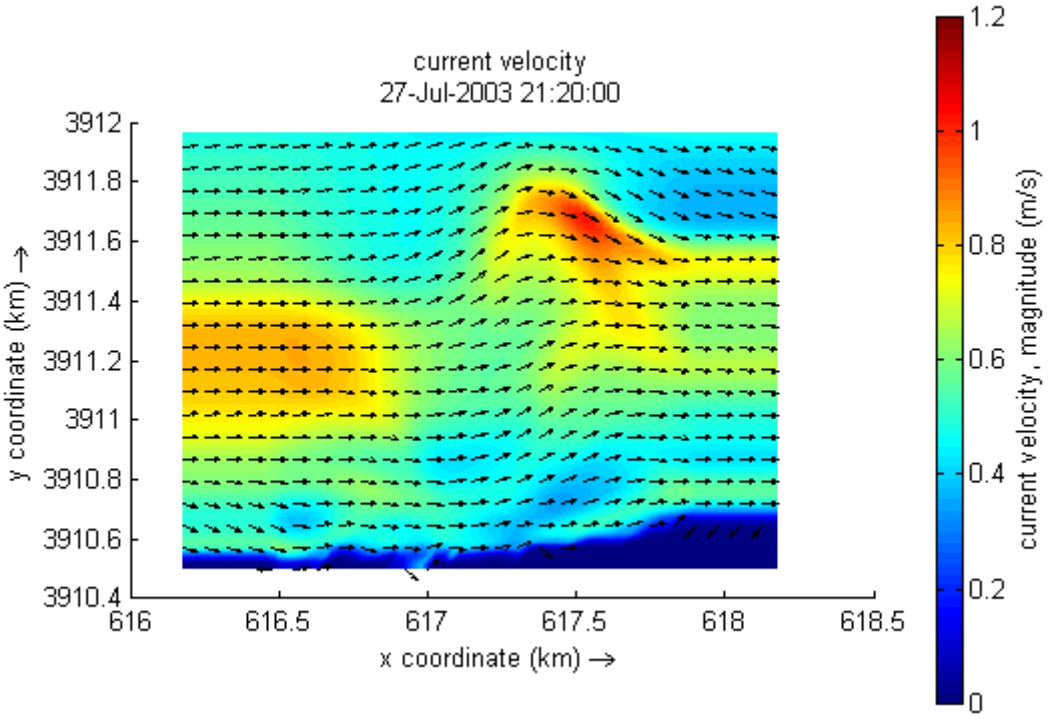

Figure 5.26: During the peak of the storm

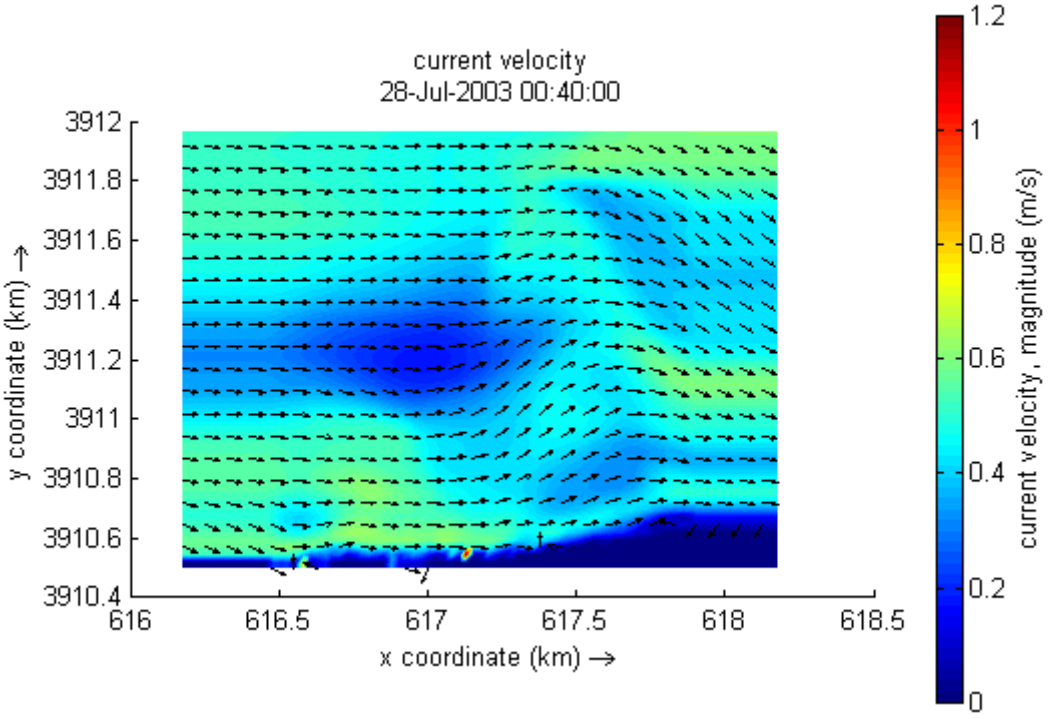

Figure 5.27: During the peak of the storm

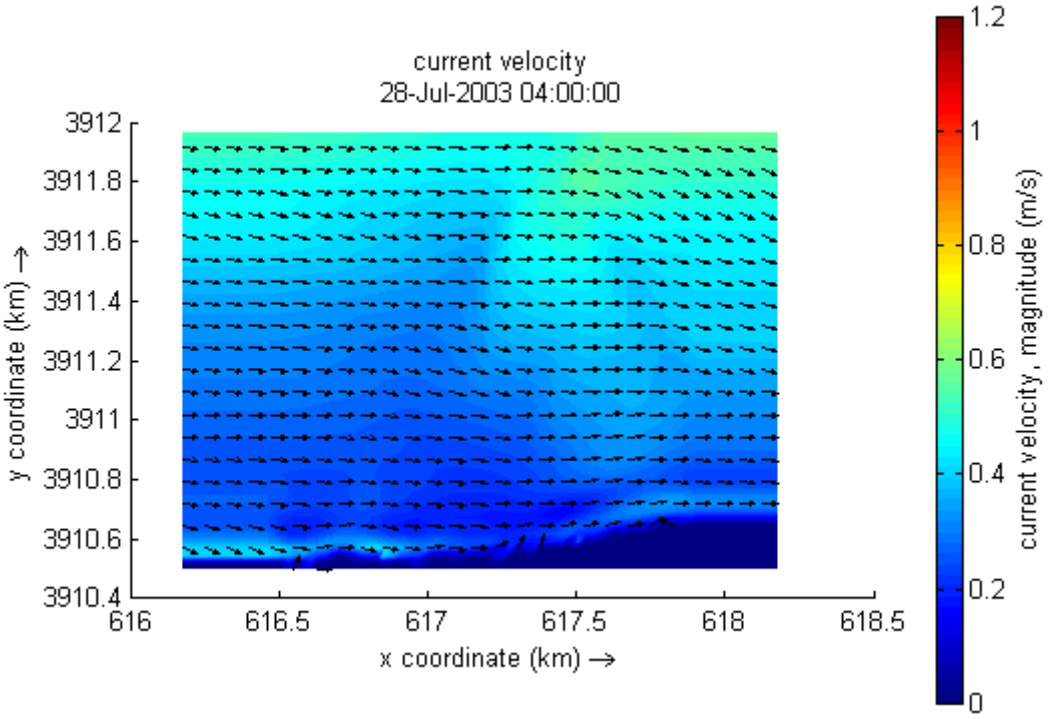

Figure 5.28: During the peak of the storm

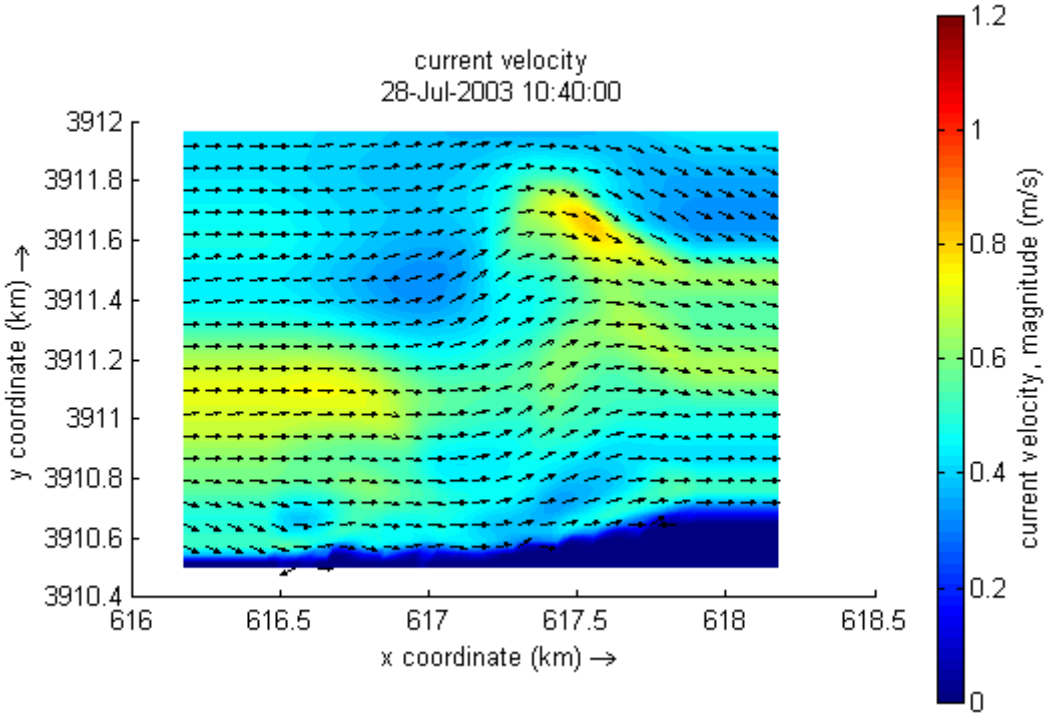

Figure 5.29: During the peak of the storm

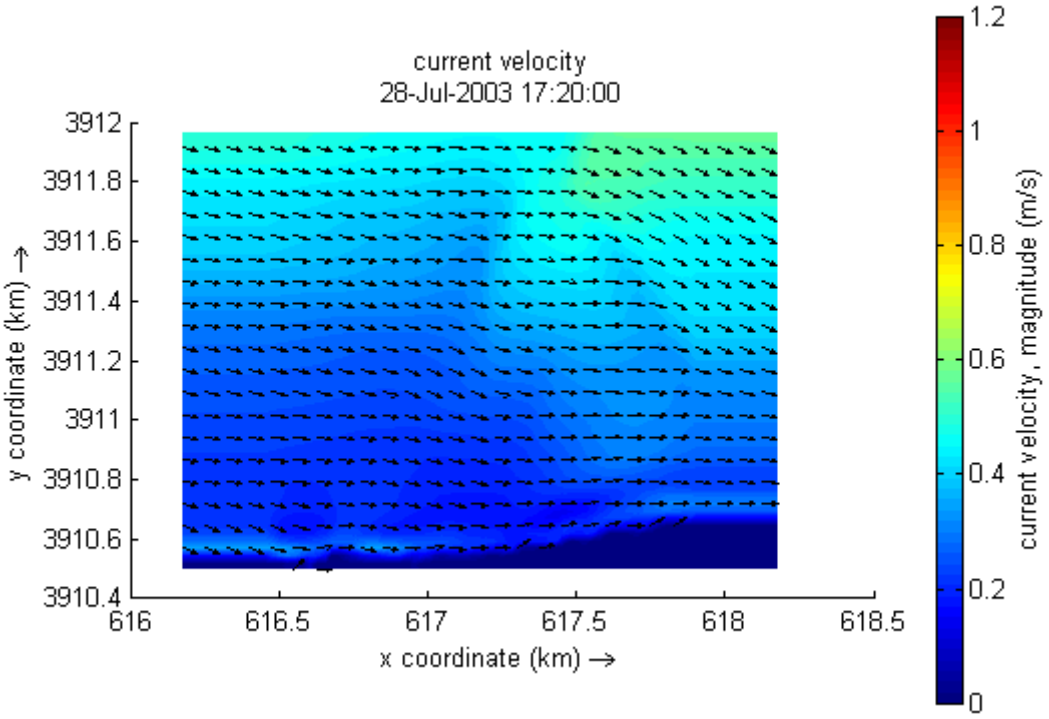

Figure 5.30: After the peak of the storm

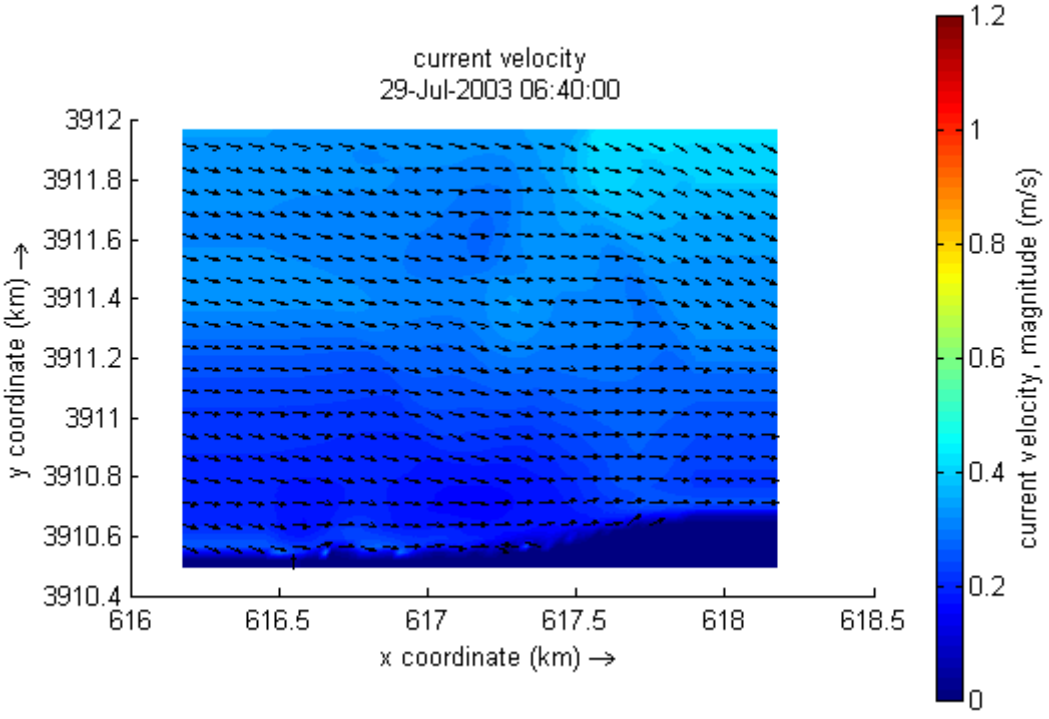

Figure 5.31: After the peak of the storm

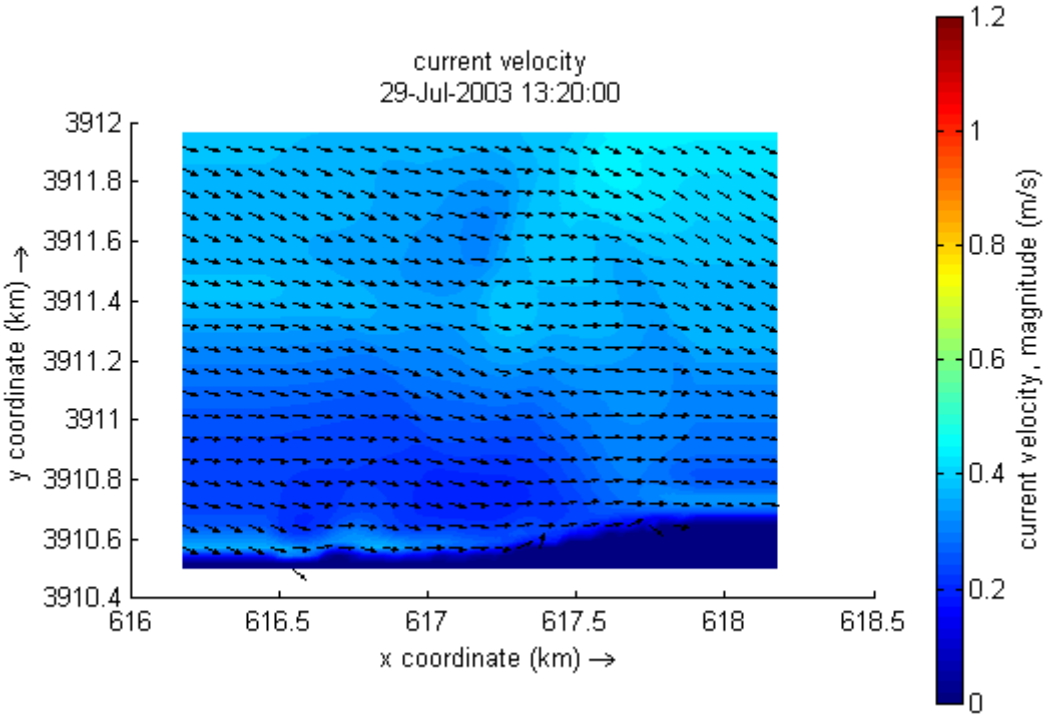

Figure 5.32: After the peak of the storm

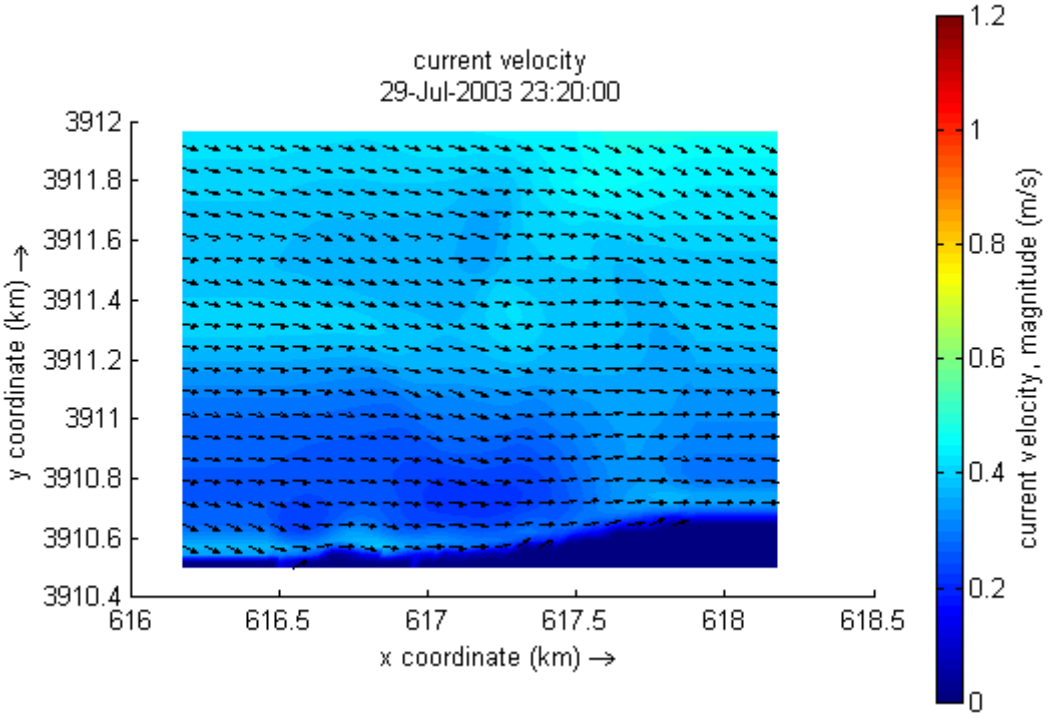

Figure 5.33: After the peak of the storm

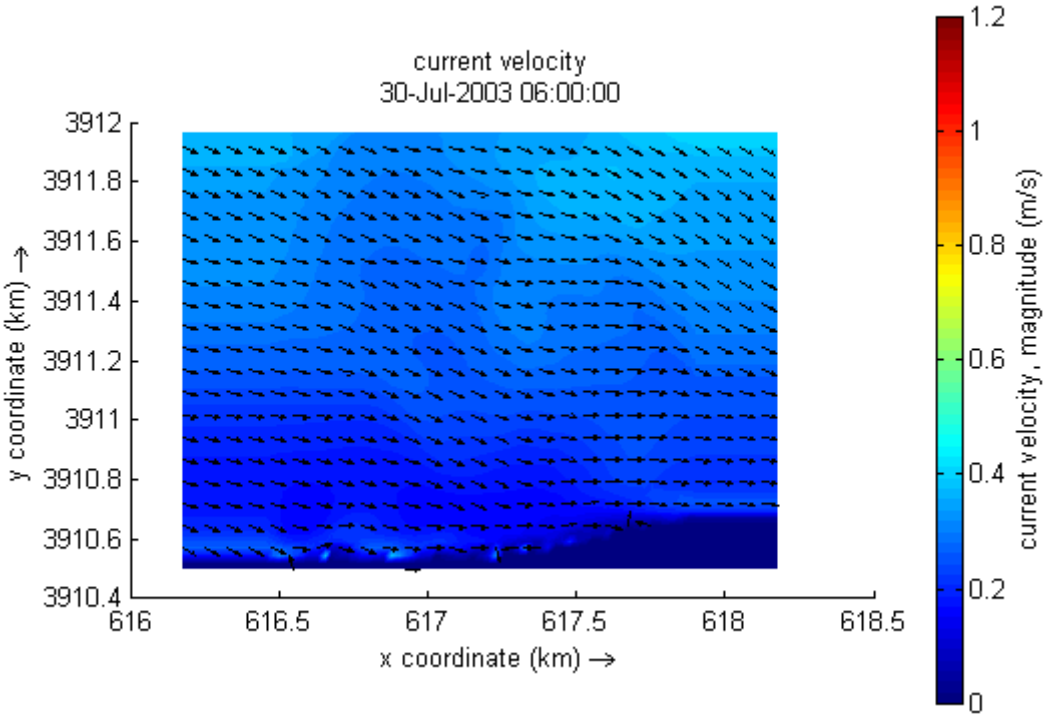

Figure 5.34: After the peak of the storm

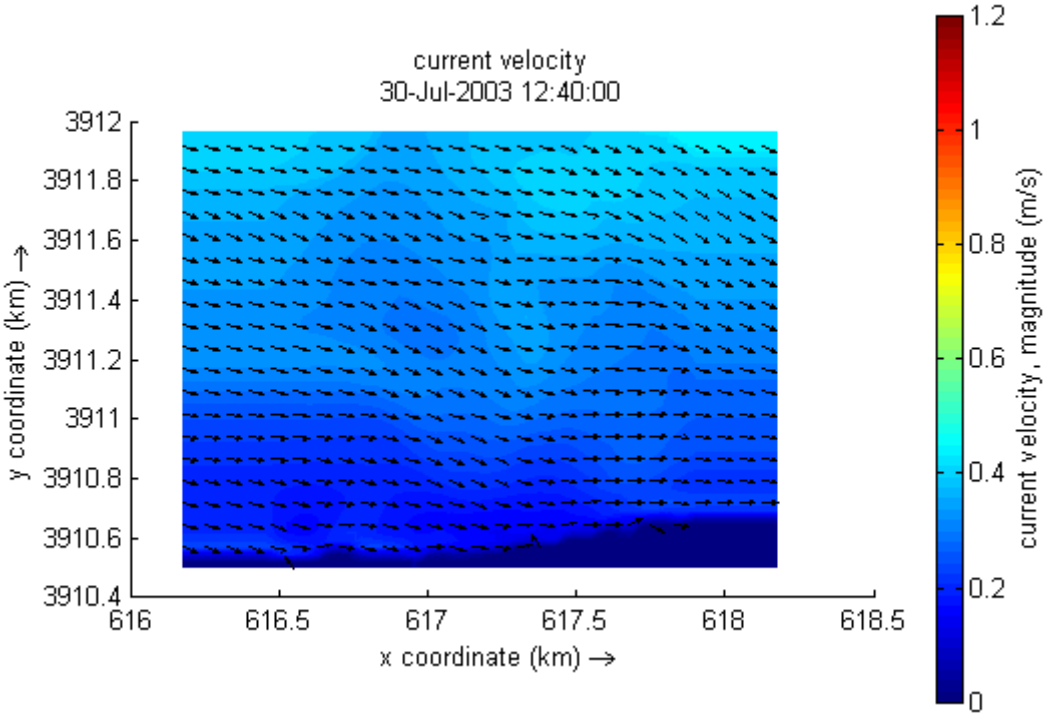

Figure 5.35: After the peak of the storm

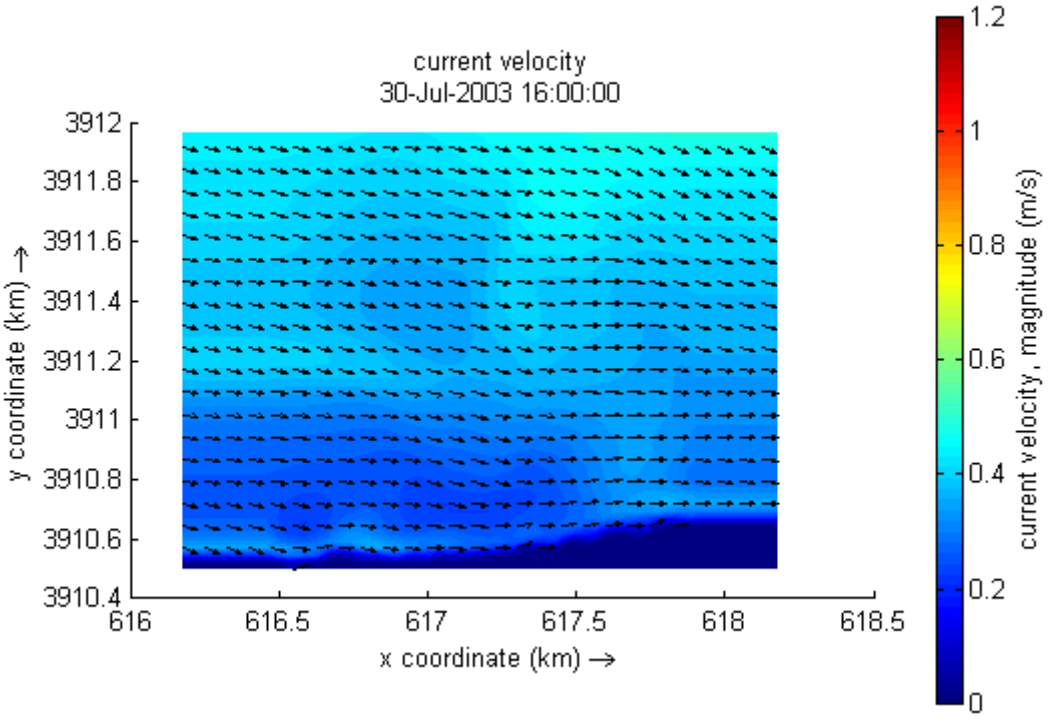

Figure 5.36: After the peak of the storm

5.3 Suspended sediment concentration

The following figures represent the contours of the suspended sediment concentration near the bed (the 12th layer corresponds to 1.8% of the depth) at selected times, during the peak of the event.

It is observed that several bars are formed, in some of which the concentration of the suspended sediment can reach the value of 1.4 kg/m^3 on the 27th of July (18:00) (U=9.18 m/s, NW) and 1.8 kg/m^3 on the 27th of July (21:20) (U = 11.1 m/s NW). On 28th of July the maximum value of the suspended sediment concentration is 1.5 kg/m^3. (figures 5.37, 5.38, 5.39, 5.40).

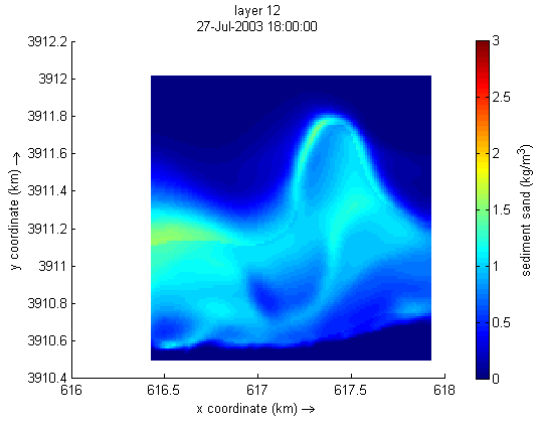

Figure 5.37: SSC 1

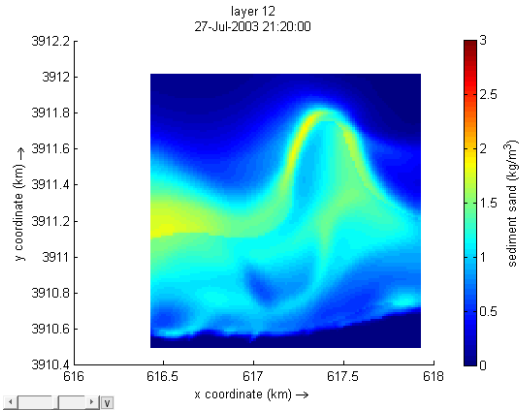

Figure 5.38: SSC 2

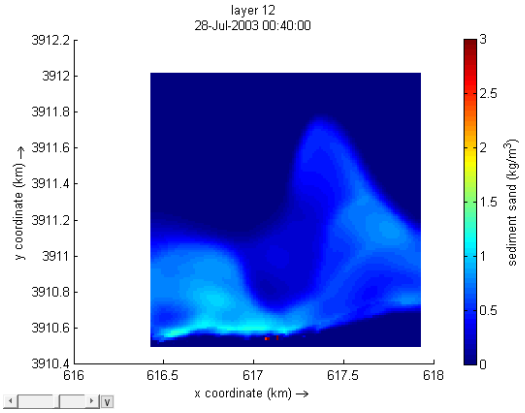

Figure 5.39: SSC 3

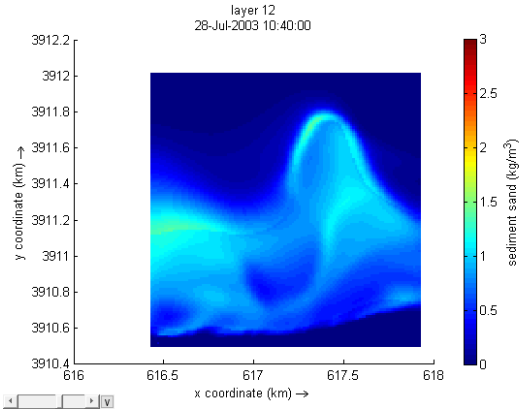

Figure 5.40: SSC 4

The following plots show the suspended sediment concentration (SSC) at the observation points G1, G2, G3 respectively, at different depths (corresponding to layers 12,10,9,8,7,1 respectively). During the peak of the Meltemi event and near the bottom, the SSC reaches the values of, approximately, 0.9 kg/m^3 at G1, 1.25 kg/m^3 at G2 and 1.62 kg/m^3 at G3 (figure 5.41,5.42,5.43). One can observe, that the SSC exceeds the value of 0.01 kg/m^3 mainly during the peak of the event, with an exception at G1 on 27th of July (09:52) that has a small peak up to 0.014 kg/m^3.

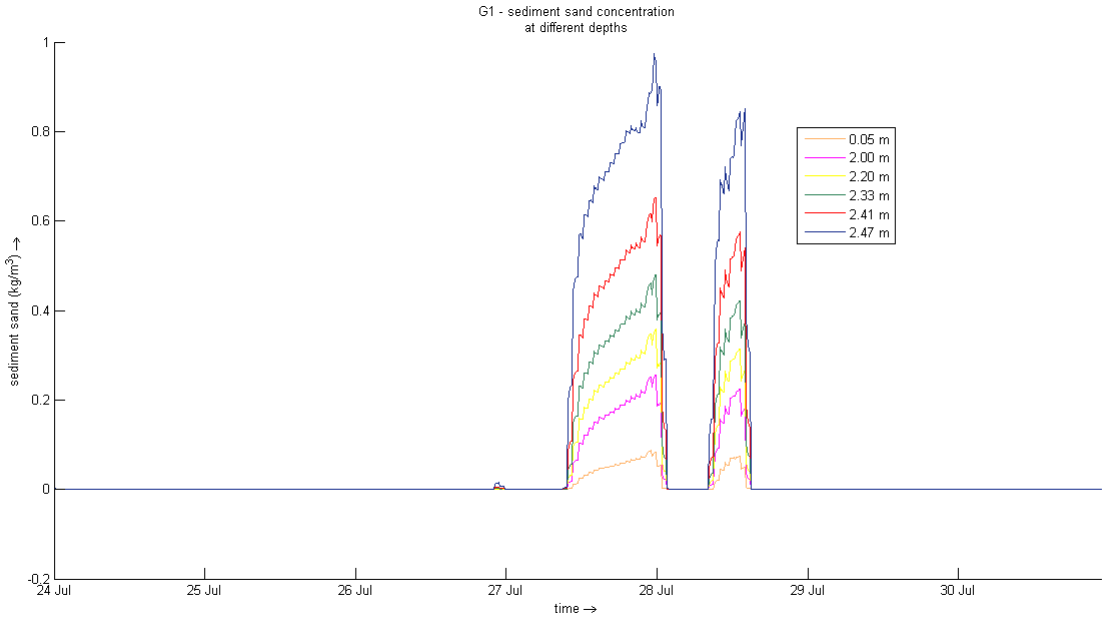

Figure 5.41: SSC at G1

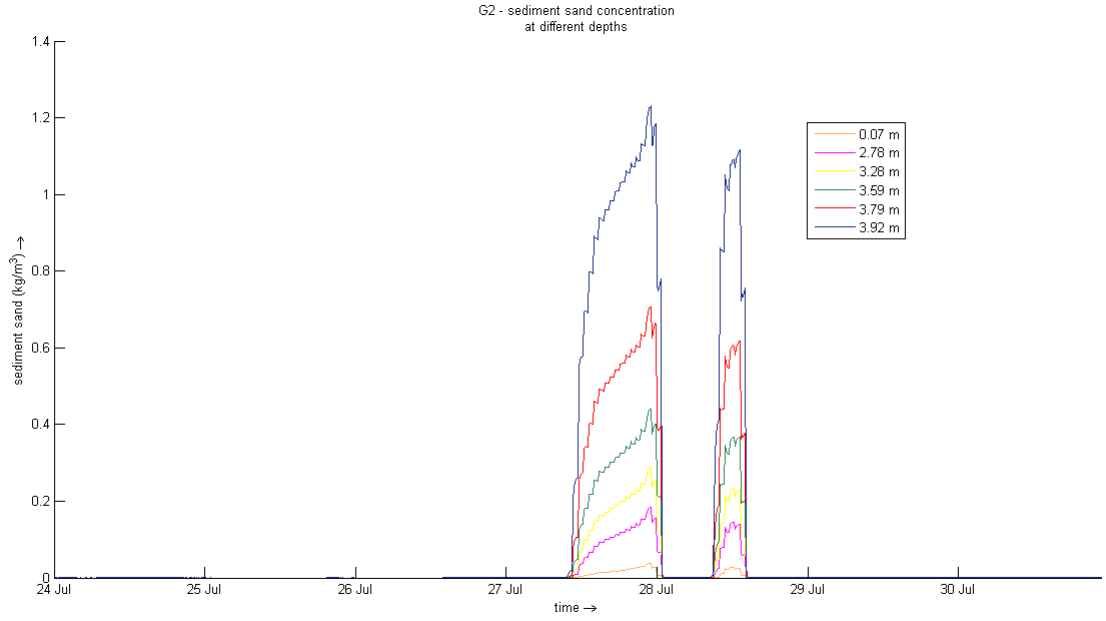

Figure 5.42: SSC at G2

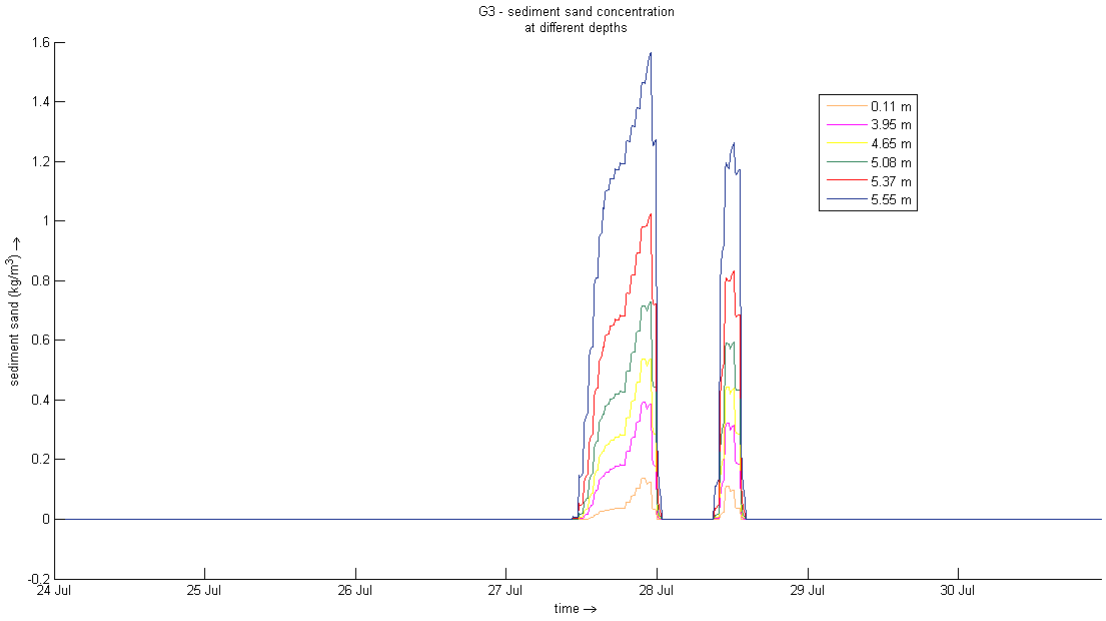

Figure 5.43: SSC at G3

From the contours of the cumulative erosion / sedimentation it is observed that before the peak of the storm, on 27th of July (11:20), when the wind velocity is around 8 m/s, the phenonenon takes place mainly in area near the shoreline with very small values. As the event reaches its peak on the 28th of July (10:40), when the wind velocity is 11 m/s the phenomenon is very intense. One can observe the various bars that are formed in several areas respresenting erosion or sedimentation. A similar pattern is repeated on the 29th of July (03:20) when the wind velocity is ≈ 7 m/s. (figure 5.44)

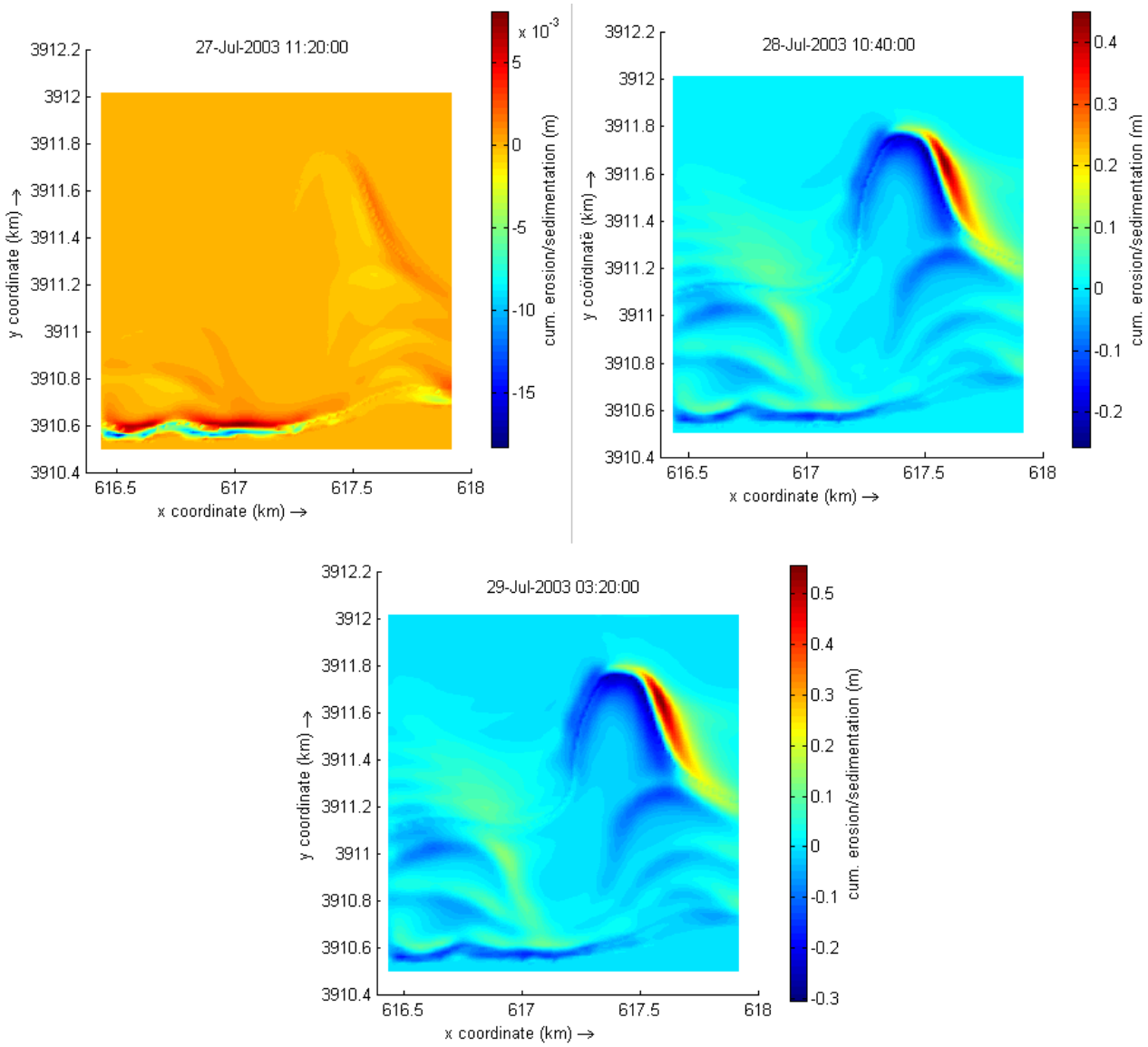

Figure 5.44: Cumulative Erosion / Sedimentation

5.4 Erosion - Sedimentation

At the observation points G1, G2, G3 an increase of sediment is observed. Particularly, at G1 we measured sedimentation ≈ 0.075m, at G2 sedimentation of ≈ 0.038m and at G3 sedimentation ≈ 0.05m.

We should comment the fact that G2 presents smaller value of sedimentation than G3. This phenomenon is related with the breaker zone and its movement.

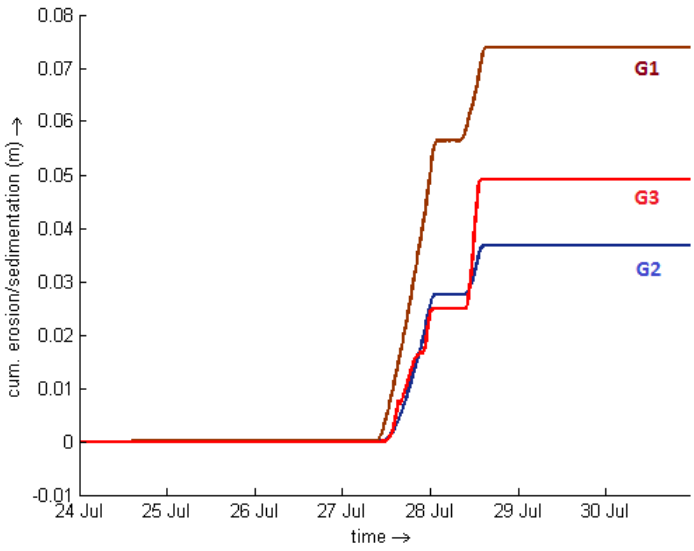

Chapter 6

Comparisons with Measurements

6.1 Significant wave height

The predicted with Delft3d model significant wave height (Hs) at the observation point G3 reaches a maximum value of 2.673m, on 27th of July (22:52, $U \approx 10m/s$) whereas measurements give the maximum value of 1.556m, on 27th of July (16:00, $U \approx 9.2m/s$). We observe a difference of 1.117m between these maximum values and a delay of approximately 7 hours for the model to reach the maximum.

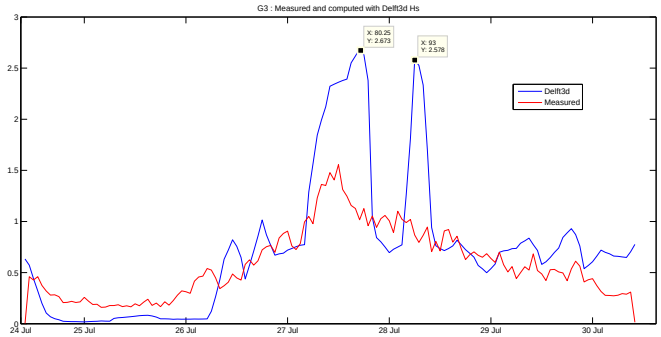

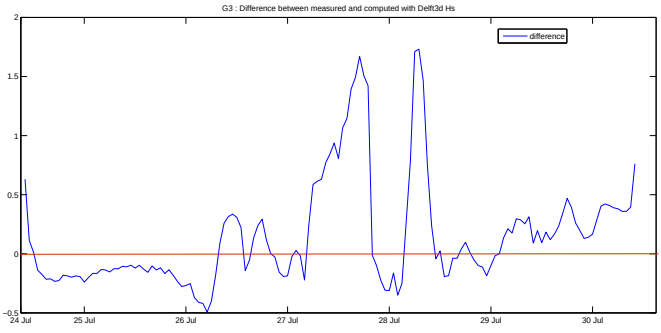

At the observation point G2, a maximum value of 1.891m is recorded by the model, on 27th of July (23:52, $U \approx 9m/s$) whereas the measured maximum value is 1.653m, on 27th of July (13:52, $U \approx 9.3m/s$). Here, the difference between the two maximum values is 0.238m with a delay of 10 hours.

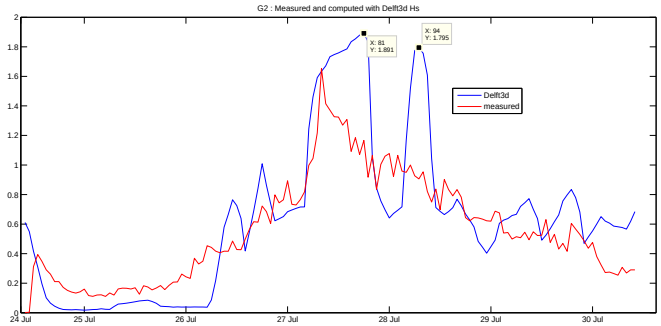

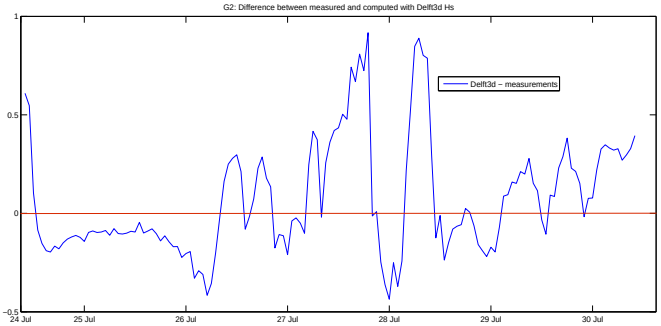

At the observation point G1, the calculated maximum value of Hs is 1.506m, on the 27th of July (22:52, $U \approx 10m/s$) whereas the measured maximum value is 1.378m, on 27th of July (16:00, $U \approx 9.2m/s$. Here, the difference between the two values is 0.128m and the time delay is approximately 8.5 hours.

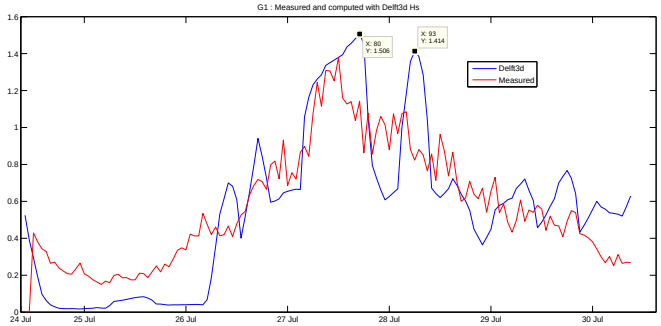

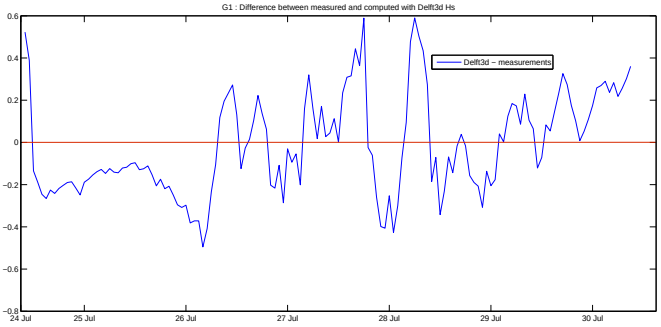

Examining the differences between the calculated and the measured Hs, we can conclude that the model underestimates the significant wave height when the wind speed is lower than $\approx 5.5 m/s$ and overestimates it for greater values of the wind speed. Also, one can observe a second maximum appearing in the simulation, that is not in the measurements. A possible explanation would be that, the transition from the maximum to the low - energy state in the simulation is faster in the reality. Also, distant breaker zones may still operating due to the continual incoming waves.

6.2 Currents

A general conclusion is that the model overestimates the mean current velocity in the area of interest. According to the measurements, the current velocity at the peak of the storm never exceeded the value of 0.2 m/s for G1 , 0.11 m/s for G2 and 0.17 m/s for G3. The threshold current velocity value is computed for the three stations and is equal to $\approx 0.36 m/s$ for G1, $\approx$ 0.38 m/s for G2 and $\approx$ 0.4 m/s for G3. However, the model estimates the current velocity in the area of interest in the range of 0.2 to 0.5 m/s, exceeding the threshold value in some areas.

6.3 Suspended sediment concentration

Since the model overestimates the significant wave height and the current velocity, a difference between the values of the suspended sediment concentration (SSC) as well is expected. Particularly, at G1 the measured SSC is $\approx 0.05 kg/m^3$, at G2 is $\approx 0.06 kg/m^3$ and at G3 is $\approx 0.37 kg/m^3$. The Delft3D model computes a sediment concentration$\approx 0.3 kg/m^3$ for G1, $\approx 0.3 - 0.45 kg/m^3$ for the G2 and $\approx 0.56 - 0.62 kg/m^3$. An explanation for this difference between the predicted and the measured sediment concentration is that in the physical domain there is coarser material than that we applied in the model.

Finally, the SSC exceeds the value of 0.01 kg/m^3 mainly during the peak of the event. The corresponding bed shear stress to the reference value of SSC = 0.01 kg/m^3 is $\tau_b = 0.15 N/m^2$ which coincides with the results from the measurements (Alexandrakis per. com.).

6.4 Bottom changes

The general view of the bottom changes from the contours of the cumulative erosion/sedimentation is very satisfying. The choice of the initial and boundary conditions led to accurate enough forecasting results regarding to the morphological conditions of the study area. Actually, the model predicts the several bars that are formed in several areas of the domain (figure 6.1).

6.5 Conclusion

The results of the simulation give very satisfactory characteristics concerning the overall view of the study area. However, it fails to accurately predict data on a grid cell level. Some improvements that can be made are to

- optimize the input parameters of the model,
- provide a more detailed bathymetry and sedimentology,
- change the resolution of the computational grids.

- testing also other models for the wave - current interaction
- apply the model to other test cases, with different data.

Figure 6.1: Bars formed in the study cite

Chapter 7

References

[**1**] Deltares, Delft3D - FLOW. Simulation of multi-dimensional hydrodynamic flows and transport phenomena, including sediments.Delft., 2013

[**2**] Deltares, Delft3D - WAVE. Simulation of short-crested waves with SWAN.Delft, 2013

[**3**] Grant, W. D. and O. S. Madsen, Combined wave and current interaction with a rough bottom. Journal of Geophysical Research 84 (C1): 17971808.1979

[**4**] Hasselmann, K., T. P. Barnett, E. Bouws, H. Carlson, D. E. Cartwright, K. Enke, J. Ewing, H. Gienapp, D. E. Hasselmann, P. Kruseman, A. Meerburg, P. Mller, D. J. Olbers, K. Richter, W. Sell and H. Walden, Measurements of wind wave growth and swell decay during the Joint North Sea Wave Project (JONSWAP). Deutsche Hydrographische Zeitschrift 8 (12).1973

[**5**] Holthuijsen, L.H., Waves in oceanic and coastal waters.Cambridge University Press,New York, USA. 2007

[**6**] Jin X.Y., Quasi-three-dimensional numerical modelling of flow and dispersion in shallow water.Ph.D. thesis, Delft University of Technology, 1993.

[**7**] Mei C. Wiley, New York., 1983

[**8**] Poulos S.E., Plomaritis T.A., Ghionis G., Nearshore wave characteristics related to a strong Etesian wind event monitored at the Gouves beach zone (Heraklion, Crete island)10th Panhellenic Symposium on Oceanography and Fisheries. Athens, Greece,2012

[**9**] Poulos S.E., Plomaritis T.A., Ghionis G., Collins M.B., Angelopoulos C., The Role of Coastal Morphology in Influencing Sea Level Variations Induced by Meteorological Forcing in Microtidal Waters: Examples from the Island of Crete (Aegean Sea, Greece) Journal of Coastal Research ,272-282,2013

[**10**] Pugh, D.T., Tides, surges and mean sea-level (reprinted with corrections). Chichester, UK, John Wiley & Sons Ltd, 486pp.1996

[**11**] Reynolds O., On the dynamical theory of incompressible viscous fluids and the determination of the criterion. Philosophical transactions of the royal society,186,1894

[**12**] Rijn, L. C. van, Sediment transport, Part II: suspended load transport. Journal of Hydraulic Engineering. 1984b

[**13**] Rijn L. C. van, Principles of Sediment Transport in Rivers, Estuaries and Coastal Seas. Aqua Publications. The Netherlands. 1993

[**14**] Ris, R. C., Spectral Modelling of Wind Waves in Coastal Areas. Communications on Hydraulic and Geotechnical Engineering, report 97-4. Delft University of Technology, Delft, The Netherlands. Ph.D. thesis.1997

[**15**] Rodi W., Turbulence Models and Their Application in Hydraulics. Taylor & Francis. 1993

[**16**] Roelvink, J. A. and D. J. R. Walstra, Keeping it simple by using complex models.In Proceedings of the 6th International Conference on Hydro-Science and Engineering. Advances in Hydro-Science and Engineering, vol. VI, page p. 12. Brisbane, Australia. 2004

[**17**] Soulsby, R. L., A. G. Davies, J. Fredse, D. A. Huntley, I. G. Jonnson, D. Myrhaug, R. R. Simons, A. Temperville and T. J. Zitman, Bed shear stresses due to combined waves and currents.In Abstracts-in-depth of the Marine Science and Technology G8-M overall workshop, Grenoble. 1993a

[**18**] Soulsby R., Dynamics of marine sands, a manual for practical applications. Thomas Telford, London. 1997

[**19**] Stelling G. S., On the construction of computational methods for shallow water flow problems.Tech. Rep. 35, Rijkswaterstaat. 1984

[**20**] Stelling, G. S. and J. J. Leendertse, Approximation of Convective Processes by Cyclic AOI methods. In M. L. Spaulding, K. Bedford and A. Blumberg, eds., Estuarine and coastal modeling, Proceedings 2nd Conference on Estuarine and Coastal Modelling, ASCE, pages771782. Tampa. 1992

[**21**] Svendsen A., Introduction to Nearshore Hydrodynamics.World Scientific. 2006

[**22**] Tsimplis, M.N., Tidal Oscillations in the Aegean and Ionian Seas: Estuarine, Coastal and Shelf Science.v. 39, no. 2, p. 201208. 1994

[**23**] Uittenbogaard, R. E., J. A. T. M. van Kester and G. S. Stelling, Model for eddy diffusivity and viscosity related to sub-grid velocity and bed topography. Tech. rep., WL — Delft Hydraulics, Delft, The Netherlands. 1998

[**24**] Uittenbogaard, R. E. and B. Van Vossen, Subgrid-scale model for Quasi-2D turbulence in shallow water. In: Shallow flows: proceedings of the international symposium. 2003

[**25**] Vossen, B. van, Horizontal Large Eddy simulations; evaluation of flow computations with Delft3D-FLOW. Tech. Rep. MEAH-197, WL — Delft Hydraulics, Delft, The Netherlands. 2000

[26] Whitham, G., Linear and nonlinear waves. Wiley, New York.1974